SULT4A1 Modulates Synaptic Development and Function by Promoting the Formation of PSD-95/NMDAR Complex

Lorenza Culotta, Paolo Scalmani, Ersilia Vinci, Benedetta Terragni, Alessandro Sessa, Vania Broccoli, Massimo Mantegazza, Chiara Verpelli

The Journal of Neuroscience

https://jneurosci.msubmit.net

JN-RM-2194-19R2

SULT4A1 modulates synaptic development and function by promoting the formation of PSD-95/NMDAR complex

Chiara Verpelli, CNR, Neuroscience Institute
Lorenza Culotta, CNR, Institute of Neuroscience
Paolo Scalmani, Fondazione IRCCS Istituto Neurologico Carlo Besta
Ersilia Vinci, CNR, Neuroscience Institute
Benedetta Terragni, U.O. of Neurophysiopathology and Diagnostic Epileptology, Foundation Istituto di Ricerca e Cura a Carattere Scientifico (IRCCS) Neurological Institute Carlo Besta
Alessandro Sessa, San Raffaele Scientific Institute
Vania Broccoli, San Raffaele Scientific Institute
Massimo Mantegazza, IPMC- CNRS UMR 7275

Commercial Interest:

SULT4A1 modulates synaptic development and function by promoting the formation of PSD-95/NMDAR complex

Lorenza Culotta[1], Paolo Scalmani[2], Ersilia Vinci[1], Benedetta Terragni[2], Alessandro Sessa[3], Vania Broccoli[1], Massimo Mantegazza[4] and Chiara Verpelli[1]

[1] CNR Neuroscience Insitute, 20129 Milan, Italy;
[2] U.O. VII Epilettologia Clinica e Sperimentale, Foundation Istituto di Ricerca e Cura a Carattere Scientifico (IRCCS) Neurological Institute Carlo Besta, 20133 Milan, Italy;
[3] Stem Cell and Neurogenesis Unit, Division of Neuroscience, San Raffaele Scientific Institute, 20132 Milan, Italy;
[4] Université Côte d'Azur (UCA), CNRS UMR 7275, Inserm, LabEx ICST, Institute of Molecular and Cellular Pharmacology (IPMC), 660 Route des Lucioles, 06560 Valbonne-Sophia Antipolis, France.

Corresponding author:
Chiara Verpelli
CNR Neuroscience Institute
Via Vanvitelli 32
20129 Milano
Italia
Email: chiara.verpelli@in.cnr.it

Number of pages: 26
Number of figures: 7
Number of words for abstract (136), introduction (585), and discussion (974).

Conflict of interest: The authors declare no competing financial interests.

Acknowledgment

This work was supported by Comitato Telethon Fondazione Onlus; contract grant number: GGP16131 to C.V, Regione Lombardia; contract grant number:"AMANDA" CUP_B42F16000440005 to C.V; Regione Lombardia NeOn Progetto "NeOn" POR-FESR 2014-2020, ", ID 239047, CUP E47F17000000009 to C.V.

Abstract

Sulfotransferase 4A1 (SULT4A1) is a cytosolic sulfotransferase, that is highly conserved across species and extensively expressed in the brain. However, the biological function of SULT4A1 is unclear. SULT4A1 has been implicated in several neuropsychiatric disorders, such as Phelan-McDermid Syndrome and schizophrenia. Here, we investigate the role of SULT4A1 within neurons development and function. Our data demonstrates that SULT4A1 modulates neuronal branching complexity and dendritic spines formation. Moreover, we show that SULT4A1, by negatively regulating the catalytic activity of Pin1 towards PSD-95, facilitates NMDAR synaptic expression and function. Finally, we demonstrate that the pharmacological inhibition of Pin1 reverses the pathological phenotypes of SULT4A1- knocked down neurons by specifically restoring dendritic spine density and rescuing NMDAR-mediated synaptic transmission. Together, these findings identify SULT4A1 as a novel player in neuron development and function by modulating dendritic morphology and synaptic activity.

SIGNIFICANCE STATEMENT

Sulfotransferase 4A1 (SULT4A1) is a brain-specific sulfotransferase highly expressed in neurons. Different evidences suggested that SULT4A1 has an important role in neuronal function and that SULT4A1 altered expression might represent a contributing factor in multiple neurodevelopmental disorders. However, the function of SULT4A1 in the mammalian brain is still unclear. Here, we demonstrate that SULT4A1 is highly expressed at postsynaptic sites where it sequesters Pin1, preventing its negative action on synaptic transmission. This study reveals a novel role of SULT4A1 in the modulation of NMDA receptor activity and strongly contributes to explaining the neuronal dysfunction observed in patients carrying deletions of *SULTA41* gene.

Introduction

Cytosolic Sulfotransferase 4A1 is member of the cytosolic sulfotransferases (SULT) superfamily, a class of enzymes that catalyze sulfonation reactions by transferring the sulfonate group from 3'-phosphoadenosine 5'-phosphosulfate (PAPS) to different endogenous and exogenous substrates (Falany et al., 2000; Negishi et al., 2001). SULT4A1 shows a remarkable degree of cross-species similarity, suggesting highly conserved biological function (Blanchard et al., 2004; Minchin et al., 2008). Of note, SULT4A1 has an atypical enzymatic domain structure, as revealed by a recent crystal structure (Allali-Hassani et al., 2007), that may affect PAPS binding and substrate specificity: in fact, no sulfonation activity has been detected with potential sulfate donors or

substrates (Falany et al., 2000; Allali-Hassani et al., 2007), suggesting SULT4A1 may not exhibit classical catalytic activity *in vivo* or that the functional enzyme may be active as a component of a multi-enzyme complex (Falany et al., 2000). Thus, in absence of any known substrate, the biological function of SULT4A1 remains unclear.

SULT4A1 tissue distribution has been examined in both humans and rodents and has been demonstrated to be predominantly expressed within the brain, although limited expression of mRNA and protein is detectable in other organs, such as kidney, lung, liver and heart tissues (Alnouti et al., 2006; Sidharthan et al., 2014). In particular, the strongest protein expression has been detected in cerebral cortex, thalamus, cerebellum, and hippocampus (Liyou et al., 2003). In mouse, Sult4a1 mRNA expression is low in fetal brains and remains nearly unchanged until postnatal day 30, after which a marked increase in expression has been observed (Alnouti et al., 2006). Consistent with this, SULT4A1 protein expression was found to increase during neuronal differentiation (Idris et al., 2019). Notably, *Sult4a1*-KO mice display severe neurological defects including tremor, rigidity and seizure and the survival of pups during postnatal development is strongly affected by loss of *Sult4a1* (Garcia et al., 2018).

A growing body of evidence supports SULT4A1 as a key player in neuronal maturation, and that loss of SULT4A1 function can contribute towards neurodevelopmental disorders. For instance, *SULT4A1* haploinsufficiency has been linked to neurological symptoms of patients with Phelan-McDermid Syndrome (PMS) (Disciglio et al., 2014; Mitz et al., 2018; Ziats et al., 2019), with *SULT4A1* deletion strongly correlated to lower developmental quotient (Zwanenburg et al., 2016). In addition, single nucleotide polymorphisms (SNP) in *SULT4A1* gene have been linked to schizophrenia susceptibility as well as severity of both psychotic and intellectual impairment, and antipsychotic treatment response (Brennan and Condra, 2005; Meltzer et al., 2008; Ramsey et al., 2011). Altogether, these findings suggest a role of SULT4A1 in neuronal development and function and altered expression as a potential contributing factor in multiple neurodevelopmental disorders.

Despite this body of supporting literature, the role of SULT4A1 within neuronal development and function remains unassessed. Our results provide evidence that SULT4A1 has a pivotal role in the regulation of neuronal morphology and synaptic activity. Our data suggests that this effect is achieved through regulation, by direct protein-protein interaction, of the peptidyl-prolyl *cis-trans* isomerase Pin1 at the synaptic level. Pin1 is an enzyme that binds to phosphorylated serine/threonine-proline motifs and catalyzes *cis*-to-*trans* isomerization of prolines (Ranganathan et al., 1997; Shen et al., 1998), notably acting to regulate synaptic strength through regulation of post-synaptic scaffolds: for instance, in excitatory synapses Pin1 has been found to downregulate glutamatergic synaptic transmission by negatively modulating PSD-95/NMDAR complex

formation (Antonelli et al., 2016). Here we demonstrate that, by sequestering Pin1, SULT4A1 facilitates the formation of the PSD-95/NMDAR complex in excitatory synapses, which is essential for NMDAR-mediated synaptic transmission and spines formation.

Materials and Methods

Constructs and virus generation

For RNA interference, a siRNA sequence targeting the *Sult4a1* C-terminus was designed following GenScript siRNA Target Finder instructions (GenScript). Nucleotide sequence: AAGTGTGACCTCACGTTTGAC. The sequence was used to generate a short hairpin RNA (indicated as sh*Sult4a1* or sh*SULT*) which was cloned into the pLVTHM-GFP vector (Wiznerowicz and Trono, 2003) using EcoRI and ClaI restriction sites. A scrambled form of shRNA was cloned into pLVTHM-GFP so to generate the control shRNA (indicated as shCtrl): nucleotide sequence GCTGAGCGAAGGAGAGAT. Previously described pFlag-SULT4A1(Mitchell and Minchin, 2009) was used for the overexpression experiments alongside pLVTHM-GFP vector as an overexpression control. Site directed mutagenesis was performed using QuikChange Lightning Site-Directed Mutagenesis Kit (Agilent Technologies) to generate a construct resistant to interference by sh*Sult4a1* (indicated as *Sult4a1*r or *Sult*r). In this construct three nucleotides (G825A, T828C, C831T) of the sh*Sult4a1* target site were altered, without changing the amino acid sequence of the resultant protein.

For viral transduction, genetically modified lentiviruses were produced as previously described (Naldini et al., 1996; Lois et al., 2002) and the production was carried out with 2nd and 3rd generation lentiviral transfer vectors.

Animals

To prepare primary neuronal rat cultures, pregnant female rats (Rattus norvegicus) of the phylum Wistar strain were purchased from Charles River (Charles River Laboratories, Calco, Italy). C57BL/6 wild-type mice were purchased from Charles River. Mice and rats were housed under constant temperature (22 ± 1°C) and humidity (50%) conditions with a 12-hour light/dark cycle and were provided with food and water *ad libitum*. All experiments involving animals followed protocols in accordance with the guidelines established by the European Communities Council and the Italian Ministry of Health (Rome, Italy).

Cell lines and transfections

HEK293T cells were cultured at 37°C and 5% CO_2 atmosphere in DMEM (ThermoFisher) supplemented with fetal bovine serum (10%, ThermoFisher), L-Glutamine (2 mM, Euroclone), PenStrep (1%, ThermoFisher). Cells were transfected using Lipofectamine 2000 (ThermoFisher) and collected 24–48 hours after transfection.

Primary neuronal cell culture

Low density rat cortical neuronal cultures were prepared from embryonic day (E) 18 rat embryos (Charles River) as previously described (Verpelli et al., 2010). Neurons were plated at 150-200 cells/mm² density on 6- or 12-well plates (Euroclone) coated with 0.01 mg/ml poly-L-Lysine (Sigma-Aldrich). Neurons were cultured in Neurobasal (ThermoFisher) supplemented with the previously described B27 (Chen et al., 2008). Cells were cultured on 6- and 12-well plates for protein biochemical analysis, whereas 12-well plates with acid-treated coverslips (VWR) were used for immunocytochemical or electrophysiological analysis. At day-in-vitro 7 (DIV7), neurons were lentivirally transduced or transfected using Lipofectamine 2000 (ThermoFisher). Biochemical, electrophysiological and morphological experiments were performed at DIV14.

PiB treatment. In order to inhibit Pin1 catalytic activity, cortical neurons were treated with PiB (diethyl-1,3,6,8-tetrahydro-1,3,6,8-tetraoxobenzol-phenanthroline-2,7-diacetate). PiB (Calbiochem) was resuspended in DMSO. As acute treatment, neurons were treated for 48h with 2.5 µM PiB and analyzed at DIV14; as chronic treatment, neurons were treated with 1 µM PiB every other day, from DIV7 to DIV14. *DTM treatment.* DTM (Calbiochem), the pharmacological inhibitor of Pin1 catalytic activity, was resuspended in DMSO. As acute treatment, cortical neurons were treated for 48h with 4 µM DTM and analyzed at DIV14.

Derivation of human iPSCs and neuronal differentiation

Human blood samples were collected according to a clinical protocol approved by the local Bioethical Committees of different medical centers. Participating individuals have been informed of the objectives of the study and signed an informed consent before inclusion in the study. Peripheral blood mononuclear cells (PBMCs) were isolated using Ficoll and growth in StemPro-34 SFM Medium (ThermoFisher), supplemented with L-Glutamine (2 mM, Euroclone), PenStrep (1%, ThermoFisher), SCF (100 ng/mL, ThermoFisher), FLT-3 (100 ng/mL, ThermoFisher), IL-3 (20 ng/mL, ThermoFisher), IL-6 (20 ng/mL, ThermoFisher). To generate human induced pluripotent stem cells (iPSCs), PBMCs were transduced with 2.0 Sendai virus particles containing four Yamanaka factors using the CytoTune-iPS Sendai Reprogramming Kit (ThermoFisher). After seven days, transduced cells were plated on cultures dishes coated with hESC-qualified matrigel

(Corning) and grown in feeder-free conditions with Essential 8 medium (ThermoFisher). Three to four weeks after transduction, iPSCs colonies were manually picked for further expansion or analysis.

For neural stem cells (NSCs) derivation, iPSCs were detached with UltraPure EDTA (ThermoFisher) and plated on matrigel-coated 6-well plates in Essential 8 medium. After 24 hours, the spent medium was replaced with PSC Neural Induction Medium (ThermoFisher) and subsequently changed every other day following manufacturer's instructions. On day 7 of neuronal induction, NSCs (P0) were harvested with StemPro Accutase (ThermoFisher) and plated on matrigel-coated plates for further expansion.

To obtain terminally differentiated neurons, proliferating NSCs were plated on matrigel-coated 6- or 12-well plates and cultured in Neurobasal medium supplemented with B27 without vitamin A (2%, ThermoFisher), PenStrep (1%, ThermoFisher), Glutamax (2mM, ThermoFisher), NT-3 (10ng/mL, Miltenyi Biotec), BDNF (10ng/mL, Miltenyi Biotec), GDNF (10ng/ml, Miltenyi Biotec), Retinoic Acid (1µM, Sigma-Aldrich) and growth for at least 40 days (Borroni et al., 2017). Half media changes were performed every 2–3 days thereafter.

Biochemical analysis

Cells or brain were lysed in pre-chilled buffered sucrose [0.32 M sucrose (Sigma-Aldrich)/ 4 mM HEPES-NaOH buffer (Sigma-Aldrich), pH 7.3, protease inhibitors (Sigma-Aldrich), phosphatase inhibitors (Roche)] and analyzed via Bradford protein assay (Bio-Rad) to assess protein concentration. For total lysate, proteins were directly solubilized in 4X loading buffer [(250 mM Tris, 40% glycerol, 0.008% bromophenol blue (all Sigma-Aldrich)]. In other cases, fractionation took place prior to solubilization to obtain a synaptosome-enriched fraction (P2), as previously published (Vicidomini et al., 2017).

For immunoblotting, primary antibodies and HRP-conjugated secondary antibodies were applied overnight (o/n) and for 1 hour, respectively. Chemiluminescence was induced using an ECL kit (GE Healthcare) and densitometry was performed using Fiji/ImageJ (US National Institutes of Health).

Immunoprecipitation assay

To evaluate the interaction between Pin1, SULT4A1 and PSD-95, primary neurons were lysed in NP-40 lysis buffer [1% NP-40, 50mM Tris pH 8.0, 150mM NaCl and protease inhibitor cocktail (all Sigma-Aldrich)] and subjected to synaptosomal fractionation as previously described (Vicidomini et al., 2017). P2 fractions were pre-cleared in NP-40 buffer for 4 hours and then incubated o/n at 4 °C with protein A-Sepharose beads (GE Healthcare, Milan, Italy) conjugated to

10 µg/ml of anti-Pin1 antibody (Santa Cruz Biotechnology) or matched control IgG (Sigma-Aldrich). The beads were then washed with 0.5% NP-40 buffer, resuspended in loading buffer, warmed at 65 °C for 10 minutes and analyzed using SDS-PAGE. Samples of pre-cleared P2 fractions were collected before immunoprecipitation and used as input signals.

Electrophysiological recordings

Whole-cell patch-clamp recordings in voltage-clamp configuration were performed at room temperature (~25 °C) on DIV14 neurons using a Multiclamp 700A amplifier and pClamp 10.5 software (Molecular Devices, Sunnyvale, CA, USA). Signals were filtered at 1 kHz and sampled at 10 kHz. Postsynaptic currents were recorded at -70 mV in an external bath solution containing (mM): 129 NaCl, 1.25 NaH_2PO_4, 35 glucose, 1.8 $MgSO_4$, 1.6 $CaCl_2$, 3 KCl and 10 HEPES, pH 7.4 with NaOH. Spontaneous excitatory postsynaptic currents (sEPSCs) were recorded in the presence of gabazine (125 µM) with an intracellular pipette solution containing (mM): 120 K-gluconate, 15 KCl, 2 $MgCl_2$, 0.2 EGTA, 10 HEPES, 20 phosphocreatine-tris, 2 ATP-Na_2, 0.2 mM GTP-Na_2, 0.1 leupeptin and 3 lidocaine N-ethyl bromide, pH 7.2 with KOH. Spontaneous inhibitory postsynaptic currents (sIPSCs) were recorded in the presence of kynurenic acid (3 mM) with an intracellular pipette solution containing (mM): 135 CsCl, 2 $MgCl_2$, 0.2 EGTA, 10 HEPES, 20 phosphocreatine-tris, 2 ATP-Na_2, 0.2 mM GTP-Na_2 and 0.1 leupeptin, 3 lidocaine N-ethyl bromide, pH 7.2 with KOH; in these conditions, the Cl^- reversal potential was 0 mV, thus allowing to record at hyperpolarized potentials (-70 mV). Signals were filtered at 1 kHz and sampled at 10 kHz. The quantification of the instantaneous frequency, the inverse of the inter-event interval, and of the amplitude of postsynaptic currents was performed on 2 minutes-long recordings with Clampfit 10.5 using a threshold search (threshold set at four times the baseline root mean square, RMS, noise).

NMDA-mediated currents (I_{NMDA}) were elicited by the perfusion of 100 µM NMDA and recorded at -70 mV with an external bath solution containing (mM): 150 NaCl, 3 KCl, 3 $CaCl_2$, 10 HEPES, 8 glucose, 0.1 D-Serine, 0.001 tetrodotoxin, 0.01 DNQX, 0.01 picrotoxin and 0.001 CGP 55845, pH 7.4 with NaOH. AMPA-mediated currents (I_{AMPA}) were elicited by the perfusion of 100 µM AMPA and recorded at -70 mV with an external bath solution containing (mM): 150 NaCl, 3 KCl, 3 $CaCl_2$, 2 $MgCl_2$, 10 HEPES, 8 glucose, 0.1, 0.001 tetrodotoxin, 0.01 D-CPP, 0.01 picrotoxin and 0.001 CGP 55845, pH 7.4 with NaOH. Internal pipette solution containing (mM): 135 CH_3O_3SCs, 8 NaCl, 0.5 EGTA, 10 HEPES, 0.3 GTP-Na_2 and 4 ATP-Mg, pH 7.2 with CsOH. NMDA and AMPA application was performed with a local fast perfusion system controlled by electronic valves (RSC-200 Rapid Solution Changer, Bio-Logic Science Instruments); the tip of a multichannel manifold was placed at a distance of 0.2 mm from the patched neuron, allowing a fast solution exchange. To

avoid drug accumulation, 10 minutes of wash out was applied after each recording. Peak I_{NMDA} and I_{AMPA} were normalized to the membrane capacitance to obtain the current densities for statistical analysis.

***In utero* electroporation, section preparation and immunohistochemistry**

In utero electroporation was employed to deliver shCtrl- and sh*Sult4a1*-expressing vectors to the ventricular RGCs of CD1 mouse embryos as previously described (Sessa et al., 2008). Briefly, uterine horns of E 13.5 pregnant dams were exposed by midline laparotomy after anesthetization with Avertin (312 mg/kg, Sigma-Aldrich). 1 µl of DNA plasmid(s) corresponding to 3 µg mixed with 0.03% fast-green dye in PBS was injected in the telencephalic vesicle using a pulled micropipette through the uterine wall and amniotic sac. 7 mm platinum tweezer-style electrodes were placed outside the uterus over the telencephalon and 5 pulses of 40 V, 50 ms in length, were applied at 950 ms intervals by using a BTX square wave electroporator. The uterus was then replaced in the abdomen, the cavity was filled with warm sterile PBS and the abdominal muscle and skin incisions were closed with silk sutures.

At post-natal day 30, GFP-positive brains were dissected for subsequent analyses. To this purpose, animals were anesthetized with an intraperitoneal injection of Avertin and perfused with 5% sucrose and 4% paraformaldehyde. Then, brains were left overnight in 4% paraformaldehyde, followed by incubation in 30% sucrose. Finally, brains were included in cryomolds with Tissue-Tek OCT compound (Sakura) and stored at −80°C until cryostat sectioning. 50 µm-thick slices were collected on polysine microscope adhesion slides (ThermoFisher) and then incubated in blocking solution (3% BSA, 10% goat serum, 0.4% Triton-X-100, diluted in PBS). Primary and fluorophore-conjugated secondary antibodies were diluted in blocking solution and applied respectively o/n at 4°C and 1 hour at room temperature. Glass coverslips were mounted on slides with Mounting Medium (VectaShield).

All procedures were approved by the Italian Ministry of Health and the San Raffaele Scientific Institute Animal Care and Use Committee in accordance with the relevant guidelines and regulations.

Immunocytochemistry

Cells were fixed in 4% paraformaldehyde, 4% sucrose in PBS [136.8 mM NaCl, 2.68 mM KCl, 10.1 mM Na_2HPO_4 and 1.76 mM KH_2PO_4, pH 7.4 (all Sigma-Aldrich)] at room temperature for 10 minutes. For colocalization analysis, neurons were fixed in 4% paraformaldehyde, 4% sucrose in PBS at room temperature for 5 minutes and then in cold methanol at -20°C for 10 minutes. Primary

antibodies were diluted in homemade gelatin detergent buffer (GDB) [30 mM phosphate buffer, pH 7.4, 0.2% gelatin, 0.5% Triton X-100, 0.8 M NaCl (all Sigma-Aldrich)] and applied o/n at 4°C. Secondary antibodies conjugate with fluorophores (Jackson ImmunoResearch Laboratories) were also diluted in GDB buffer and applied for 1h. DAPI staining (ThermoFisher) was carried out at a final concentration of 0.5 μg/ml. Coverslips were mounted on pre-cleaned microscope slides using Mowiol mounting medium (Osborn and Weber, 1982).

Image acquisition and processing

Confocal images were obtained using LSM 510 Meta confocal microscope (Carl Zeiss) with Zeiss 63X, 40X or 20X objectives at a resolution of 1024x1024 pixels. Images represent averaged intensity Z-series projections of 2-7 individual images taken at depth intervals of around 0.45 μm. Secondary and tertiary dendrites with comparable length and width were selected for dendritic spine analyses. Dendritic spine analysis was performed as described in Verpelli et al (Verpelli et al., 2011a) but using Fiji/ImageJ software (US National Institutes of Health) for the quantification. For colocalization analysis, measurements were performed using MetaMorph software (Universal Imaging, West Chester, PA). For neuronal arborization analysis, primary and secondary dendrites were measured manually after identifying the points of intersection. The dendrites originating from the cell body were considered as primary dendrites, while all the dendrites originating from the primary dendrites at the point of intersection were considered as secondary dendrites. Sholl analysis and total dendrites length quantification were performed using Fiji/ImageJ software. Branching points intersections were counted and plotted against distance from the soma.

Antibodies

The following primary antibodies were used: mouse anti-β-actin (Sigma-Aldrich, A5316), mouse anti- βIII-tubulin (Sigma-Aldrich, MAB1637), mouse anti-$GABA_AR\alpha1$ (NeuroMab, 75-136), mouse anti-GAD65 (Synaptic System, 198 111), mouse anti-GAD67 (Santa Cruz Biotechnology, sc-28376), mouse anti-GFP (Roche, 11814460001), rabbit anti-GluA1 (Millipore, AB1504), mouse anti-GluA2 (NeuroMab, 75-002), mouse anti-GluN1 (BD, 556308), mouse anti-GluN2A (NeuroMab, 75-288), rabbit anti-GluN2B (Millipore, 06-600), mouse anti-MAP2 (Abcam, ab11268), rabbit anti-mGlu5 (Millipore, AB5675), mouse anti-Nestin (Millipore, MAB5326), mouse anti-NLGN1 (NeuroMab, 75-160), mouse anti-Oct4 (Santa Cruz Biotechnology, sc-5279), mouse anti-Pin1 (Santa Cruz Biotechnology, sc-46660), mouse anti-PSD-95 (NeuroMab, 75-028), rabbit anti-PSD-95 (Cell Signaling, D27E11), rabbit anti-Sox2 (Proteintech, 11064-1-AP), rabbit anti-SULT4A1 (Proteintech, 12578-1-AP), rabbit anti-VGAT (Synaptic System, 131 003).

All HRP- and fluorophore-conjugated secondary antibodies were purchased from Jackson ImmunoResearch Laboratories.

Experimental Design and Statistical Analysis

Data are expressed as Mean ± SEM or percentage, analyzed for statistical significance, and displayed by Prism 7 software (GraphPad, San Diego, CA). Shapiro-Wilk test or D'Agostino-Pearson tests were applied to test the normal distribution of experimental data. Normal distributions were compared with *t*-test or ANOVA with appropriate *post-hoc* test. Non-normal distributions were compared with the non-parametric Mann-Whitney test or Kruskal-Wallis test with appropriate *post-hoc* test, as indicated. The accepted level of significance was $P \leq 0.05$.

Statistical analyses for electrophysiological experiments were performed with OriginPro software. Distributions of cumulative probabilities were compared with the Kolmogorov-Smirnov test.

No statistical methods were used to predetermine sample sizes, but sample sizes were chosen to be similar to those reported in previous publications.

In the figures, we show the mean as estimator of central tendency also when we have used a non-parametric test, for consistency with other figures in the paper and because it is more intuitive to compare the mean values.

Results

Sulfotransferase 4A1 expression is increased during brain maturation

SULT4A1 is a brain-specific sulfotransferase highly conserved among vertebrate, that appears to have a particularly strong expression in distinct areas of the cerebral cortex (e.g. prefrontal cortex), cerebellum (e.g. neuronal stroma) and brainstem (e.g. hypoglossal nucleus) (Liyou et al., 2003). To investigate SULT4A1 expression during neuronal maturation, we analyzed protein lysates harvested from rat cortical neurons at 1, 7, and 14 days in vitro (DIV1, 7 and 14). SULT4A1 expression was almost undetectable at DIV1 and increased during the neuronal maturation (Fig. 1A; DIV1: 0.03±0.01; DIV7: 0.18±0.02; DIV14: 0.38±0.03). Then, SULT4A1 expression was evaluated *in vivo* during mouse brain development. Western blot (WB) analysis showed that SULT4A1 protein levels increased from post-natal day (P) 0 to P30. Moreover, high levels of SULT4A1 were maintained also in adult mice (P60), suggesting an important role of SULT4A1 both during brain maturation and adulthood (Fig. 1B P0: 0.12±0.03; P7: 0.48±0.09; P14: 0.66±0.11; P21:0.91±0.23; P30: 0.79±0.15; P60: 1.0±0.3). SULT4A1 is known to have particularly strong expression in the brain but, to date, the current knowledge of SULT4A1 area-specific expression is restricted to

human and rat tissues (Liyou et al., 2003). In order to assess the tissue distribution in adult mouse brain, WB analysis of total lysates of hippocampus (H), striatum (S), cerebral cortex (Cx) and cerebellum (Cb) was performed on 2-month-old male mice. SULT4A1 was found to be highly expressed in all analyzed areas (Fig. 1C; H: 0.71±0.05; S: 0.93±0.06; Cx: 1.19±0.03; Cb: 1.33±0.10). Finally, no significant difference in area-specific protein expression was observed between male and female animals (Fig. 1D; H: M 0.69±0.12, F 0.67±0.12; S: M 0.80±0.12, F 0.85±0.13; Cx: M 0.87±0.10, F 1.05±0.14; Cb: M 1.16±0.20, F 1.07±0.24). The immunostaining of cortical neurons revealed a localization of SULT4A1 to neuronal cell bodies and dendrites (Fig. 1E).

To determine SULT4A1 protein expression in human neurons, human induced pluripotent stem cells (iPSCs) were differentiated into Nestin-positive Neural Stem Cells (NSCs) and subsequently into neurons (Fig. 1F) and analyzed for SULT4A1 protein levels during differentiation. Human SULT4A1 expression was found to be increased during differentiation from NSCs (day 0) to mature neurons (day 40) (Fig.1G day 0: 0.23±0.08; day 10: 0.14±0.06; day 20: 0.63±0.02; day 30: 1.57±0.1; day 40: 2.04±0.17).

SULT4A1 silencing reduces neuronal arborization and dendritic spine density

In order to evaluate the impact of SULT4A1 on neuronal morphogenesis, specific shRNAs for *Sult4a1* (sh*Sult4a1*) were designed and validated in *Sult4a1*-transfected HEK cells (Extended data: Figure 2-1 A). shRNA #1 was chosen for further analysis due to its stronger effect on *Sult4a1* protein level, and therefore indicated as sh*Sult4a1*. To confirm the specificity of sh*Sult4a1* silencing activity, sh*Sult4a1* was expressed together with a construct resistant to interference (*Sult4a1r*) and restoration of *Sult4a1* protein level was verified (Extended data: Figure 2-1 B).

To assess the role of SULT4A1 in early neuronal development, cortical neurons were transfected at DIV7 with sh*Sult4a1* or control scrambled shRNA (shCtrl) (Fig. 2A). Dendrite morphology of transfected neurons was then evaluated by Sholl analysis at DIV14 (Fig. 2B). *Sult4a1* silencing resulted in a simplification of neuronal branching, indicated by the reduction of branching points, primary dendrites, secondary dendrites and total dendrites length (Fig. 2B-E). These morphological alterations were prevented by co-transfection of sh*Sult4a1* with *Sult4a1r* (Fig 2A-E) (Branching points, condition factor: $P<0.0001$; condition by distance interaction: $P<0.0001$. Primary dendrites, shCtrl: 7.30±0.39, sh*Sult4a1*: 4.70±0.43, *Sult4a1*r: 7.3±0.45. Secondary dendrites, shCtrl: 11.60±0.94, sh*Sult4a1*: 6.26±0.51, *Sult4a1*r: 9.55±0.65. Total dendrites length, shCtrl: 1430.21±132.93, sh*Sult4a1*: 644.78±61.86, *Sult4a1*r: 1429.04±140.90).

The analysis of dendritic spine morphology revealed that *Sult4a1*-knocked down neurons exhibit a significant decrease in spines number (Fig. 2I) (Spines number shCtrl: 4.07±0.18, sh*Sult4a1*: 2.96±0.24, *Sult4a1*r: 4.05±0.36), but the morphology of the remaining spines is unchanged (Fig. 2G-H) (Spines length, shCtrl: 1.97±0.10, sh*Sult4a1*: 1.90±0.10, *Sult4a1*r: 1.86±0.09; Spines width: shCtrl: 1.03±0.05, sh*Sult4a1*: 1.04±0.05, *Sult4a1*r: 1±0.03). A slight increase of the number of spines with filopodia-like morphology was observed in *Sult4a1*-knocked down neurons (Fig. 2J). Co-transfection of sh*Sult4a1* with *Sult4a1*r prevented these morphological alterations (Fig. 2A-J).

To further confirm the role of SULT4A1 in modulating dendritic arborization and spine morphology *in vivo*, *in utero* electroporation was performed on wild type mouse cortical neurons with sh*Sult4a1* or shCtrl. Brain slices from 1-month-old electroporated animals were analyzed by confocal microscopy to measure dendritic complexity (Fig. 2K). Sholl analysis showed that, as *in vitro*, the number of branching points is decreased in cortical neurons following *Sult4a1* knockdown (Fig. 2L; condition factor: P=0.0112, condition by distance interaction: P=0.0629). Moreover, *Sult4a1* knockdown caused a significant reduction of total dendrites length (Fig. 2M shCtrl: 421.4±28,35, sh*Sult4a1*:292.86±40.42).

The reduction in spines number was confirmed, *in vivo*, in sh*Sult4a1* electroporated cortical neurons (Fig. 2N-R) (Spines number shCtrl:12±0.37, sh*Sult4a1*:10.81±0.5; Spines length, shCtrl:1.23±0.12, sh*Sult4a1*: 1.33±0.04; Spines width: shCtrl: 0.7±0.1, sh*Sult4a1*: 0.56±0.01).

To assess the role of SULTA4A1 dosage in modulating neuronal morphology, neurons were transfected at DIV7 with GFP or GFP plus *Sult4a1* and stained at DIV14 with anti-SULT4A1 antibody to identify *Sult4a1*-overexpressing neurons (Fig. 3A). *Sult4a1* overexpression led to an overall redistribution of the branching points along the dendritic tree compared to wild type neurons: neurons overexpressing *Sult4a1* presented fewer branching points close to the soma (<50 µm from soma) and an increased number of distal branching points (>100 µm from soma) (condition by distance interaction: P=0.0005) (Fig. 3B), suggesting a reorganization of neuronal arborization. However, the number of primary dendrites (GFP: 7.7±0.36, Overexpression: 8.38±0.43), secondary dendrites (GFP: 11.7±0.76, Overexpression: 13.05±0.86) and the total dendrites length (GFP: 1513.0±70.64, Overexpression: 1753.32±139.04) were equal in the two conditions (Fig. 3C-E). Interestingly, cortical neurons overexpressing *Sult4a1* displayed a significant decrease in dendritic spine density (Fig. 3I, Spines number: GFP 4.26±0.22, Overexpression 3.61±0.18), correlated to considerably longer spine morphology, as compared to wild type neurons, suggesting an immature phenotype (Fig. 3G, spine length, µm: GFP 1.95±0.08, Overexpression 2.71±0.19; Fig.3H, spine width, µm: GFP 1±0.03, Overexpression: 1.02±0.03)

(Fig. 3F-I). Indeed, we found an increase in spines with filopodia-like morphology in neurons overexpressing *Sult4a1* (Fig 3J).

These data demonstrate an important role for SULT4A1 in the regulation of both dendritic complexity and dendritic spine morphology.

Functional modifications induced by SULT4A1 knockdown.

Considering that SULT4A1 knockdown affected dendritic arborization and spine density, the effect of SULT4A1 silencing on the expression of relevant synaptic proteins was further investigated.

First, a lentiviral plasmid expressing sh*Sult4a1* was validated as effective in reducing the levels of endogenous SULT4A1 protein in cortical neurons (Fig. 4A; Ni: 1; shCtrl: 0.94±0.02, sh*Sult4a1*: 0.08±0.02). Immunoblotting analysis of total lysates showed a significant decrease in NMDA receptor subunit GluN1 expression (shCtrl: 1, sh*Sult4a1*: 0.81±0.06) and, simultaneously, a considerable increase of GAD65 protein level (shCtrl: 1, sh*Sult4a1*: 1.38±0.16) in sh*Sult4a1*-infected neurons (Fig. 4B).

To explore whether SULT4A1 silencing functionally affected glutamatergic and GABAergic activity, spontaneous post-synaptic currents (sPSCs) were recorded from shCtrl or sh*Sult4a1* transfected neurons. SULT4A1 knockdown neurons displayed a significant reduction of spontaneous excitatory postsynaptic currents (sEPSC) frequency and amplitude, reflected by the leftward shift of the cumulative probability curves and by the reduction of the median value (Instantaneous frequency: shCtrl: median 30.0 Hz, mean±SEM, 69.6±1.3 Hz, sh*Sult4a1*: 16.9 Hz, 62.9±1.6 Hz; Amplitude shCtrl 16.1 pA, 18.6±0.2pA; sh*Sult4a1*: 12.9 pA, 16.5±0.4 pA) (Fig. 4C). Moreover, an increase of the frequency of spontaneous inhibitory postsynaptic current (sIPSC) was observed as a reduction of low frequency events (0.5-5Hz range), reflected by the rightward shift of the lower part of the cumulative probability curve, whereas the median value displayed a non-significant trend toward increased frequency (shCtrl: 7.0 Hz, 16.8±0.6 Hz; sh*Sult4a1*: 5.5 Hz, 17.3±0.5 Hz) (Fig. 4D). Amplitude of sIPSC was instead significantly increased, reflected by the rightward shift of the cumulative probability curve and by the increase of the median value sIPSCs (shCtrl: 31.8 pA, 38.7±0.7pA, sh*Sult4a1*: 35.5 pA, 41.8±0.7 pA). Consistently with data of expression levels, the results of the analysis of sPSCs suggest that SULT4A1 knockdown induces a decrease of glutamatergic synaptic activity and an increase of GABAergic synaptic activity.

SULT4A1 modulates NMDAR activity preventing Pin1-PSD-95 interaction

Our biochemical data indicate that the knockdown of SULT4A1 in neurons causes a significant decrease of GluN1. Therefore, total NMDAR-mediated currents (I_{NMDA}) in neurons transfected with

437 sh*Sult4a1* were assessed. A specific reduction of I_{NMDA} was observed, quantified as peak current
438 density. This reduction was prevented by co-transfecting the sh*Sult4a1* with the *Sult4a1r* (shCtrl,
439 pA/pF: 28.3±1.9; sh*Sult4a1*: 20.7±1.4 *Sult4a1*r: 28.9±2.7) (Fig. 5A). Moreover, we measured total
440 AMPAR-mediated currents (I_{AMPA}). Our results showed a slight but not significant reduction in
441 neurons transfected with sh*Sult4a1* (shCtrl, pA/pF: 15.3±1.1; sh*Sult4a1*: 12.8±2.4 *Sult4a1*r:
442 18.9±3.5) (Fig. 5B), suggesting that SULT4A1 knockdown caused a specific NMDARs impairment
443 in synapses.
444 To elucidate whether the decreased I_{NMDA} was associated with a reduced recruitment of NMDARs
445 clusters at synapses, immunocytochemical experiments were performed on cortical neurons co-
446 labeled for PSD-95 and GluN1 (Fig.5C). We found a significant reduction of the number of GluN1
447 clusters per 10 µm of dendrite (shCtrl: 7.23±0.33, sh*Sult4a1*: 5.22±0.33) and a reduction of
448 GluN1/PSD-95 colocalization (% of colocalization, shCtrl: 78.7±3.41, sh*Sult4a1*: 55.88±3.90) in
449 *Sult4a1* knockdown neurons (Fig. 5E-F). No difference in the number of PSD-95 clusters was
450 detected (shCtrl: 8.04±0.41, sh*Sult4a1*: 7.06±0.47) (Fig. 5D).
451 Immunoblot analysis confirmed lower levels of GluN1 (shCtrl: 1; sh*Sult4a1*: 0.83±0.02) and, albeit
452 not statistically significant, a trend towards a reduction of GluN2B (p=0.1084, shCtrl: 1; sh*Sult4a1*:
453 0.7852±0.10) in synaptosomal preparations derived from *Sult4a1*-deficient neurons (Fig. 5G).
454 Peptidyl-prolyl *cis-trans* isomerase Pin1 is highly expressed at excitatory synapses, where it exerts
455 a negative action on synaptic transmission by interfering with the PSD-95/GluN2B complex
456 formation (Antonelli et al., 2016). Since it has been demonstrated that SULT4A1 is able to
457 specifically interact with Pin1 with the phosphoserine/threonine-proline motifs in its N-terminus
458 (Mitchell and Minchin, 2009), the effects of SULT4A1 knockdown on synaptic expression of Pin1
459 was analyzed. A significant increase in Pin1 synaptic levels was evidenced by immunoblot analysis
460 of synaptosomal preparations derived from SULT4A1-deficient neurons (shCtrl: 1; sh*Sult4a1*:
461 1.17±0.02) (Fig. 5G).
462 To test if SULT4A1 directly affects the Pin1-PSD-95 interaction at synaptic levels, endogenous
463 Pin1 was immunoprecipitated from synaptosomal preparations using an anti-Pin1 antibody, and the
464 co-precipitated PSD-95 was visualized using an anti-PSD-95 antibody (Fig. 5H). With SULT4A1
465 silencing, the amount of PSD-95 co-precipitated by Pin1 was increased by 40% as compared to
466 SULT4A1 expressing neurons (shCtrl: 0.83±0.10; sh*Sult4a1*: 1.19±0.10). Thus, these results
467 suggest that SULT4A1 is able to recruit Pin1 and, preventing its interaction with PSD-95, facilitates
468 the formation of PSD-95/NMDAR complex. In conclusion, our data suggest that the reduction of
469 NMDAR-mediated currents in SULT4A1-knocked down neurons is mediated by the increased
470 interaction of Pin1 with PSD-95 in excitatory synapses.

Reversal of morphological and functional deficits via Pin1 inhibition.

As synaptic level of Pin1 was found to be significantly increased following SULT4A1 knockdown, the role of Pin1 catalytic activity was assessed as a potential mechanism underlying altered glutamatergic transmission. The selective Pin1 inhibitor, PiB, was employed to inhibit Pin1 activity in SULT4A1 knockdown neurons.

Cortical neurons transfected with sh*Sult4a1* or shCtrl at DIV7 were acutely treated with 2.5 µM PiB or vehicle (DMSO) at DIV12 for 48 hours. Acute treatment with PiB resulted in an increase in peak current density in SULT4A1-knocked down neurons, while no significant effect was observed in neurons transfected with shCtrl. (pA/pF, shCtrl vehicle: 33.1±3.3; shCtrl PiB: 29.8±3.5; sh*Sult4a1* vehicle: 22.2±1.2; sh*Sult4a1* PiB: 32±2.6) (Fig. 6A). A similar result was observed by acute treatment with 4 µM DTM, an additional Pin1 chemical inhibitor (Tatara et al., 2010) (pA/pF, shCtrl vehicle: 29.0±4.7; shCtrl DTM: 30.8±7.1; sh*Sult4a1* vehicle: 22.2±3.5; sh*Sult4a1* DTM: 42.7±7.7) (Fig. 6B). Thus, Pin1 inhibition can revert NMDA currents alteration induced by SULT4A1 loss of function.

Additionally, the effect of Pin1 inhibition on dendritic spine density was investigated. Acute treatment with PiB was able to restore the number of dendritic spines in SULT4A1-knocked down neurons to levels comparable to that of control neurons (Spines number, shCtrl vehicle: 5.67±0.30; shCtrl PiB: 6.12±0.42; sh*Sult4a1* vehicle: 4.33±0.20; sh*Sult4a1* PiB: 5.82±0.30) (Fig. 6C). Spines number was also rescued by acute treatment with the second Pin1 inhibitor, DTM (Spines number, shCtrl vehicle:6.78±0.25; shCtrl DTM: 7.6±0.5; sh*Sult4a1* vehicle: 4.8±0.37; sh*Sult4a1* DTM: 7.8±0.7) (Fig. 6D).

To revert dendritic arborization deficits, sh*Sult4a1*- and shCtrl- transfected neurons were treated every other day with 1 µM PiB or 4 µM DTM or vehicle, starting at DIV7. However, chronic treatment with PiB nor DTM had any significant effect on neuronal branching (PiB treatment: shCtrl vehicle vs PiB: treatment factor P=0.4881, treatment by distance interaction P=0.9999; sh*Sult4a1* vehicle vs PiB: treatment factor P=0.3740, treatment by distance interaction: P=0.9671. DTM treatment: shCtrl vehicle vs DTM: treatment factor P=0.0743, treatment by distance interaction P=0.9021; sh*Sult4a1* vehicle vs DTM: treatment factor P=0.6666, treatment by distance interaction: P=0.0886) (Fig. 7A-F).

These results suggest that SULT4A1, through direct interaction with Pin1 in dendritic spines, plays a novel role in regulating dendritic spine maturation and synaptic transmission.

Discussion

SULT4A1 is a cytosolic sulfotransferase predominantly expressed in the brain and emerging as a genetic factor in a variety of neurodevelopmental diseases. However, the functional role of SULT4A1 within neuronal development is largely unknown since no substrate nor biological functions have been identified yet. SULT4A1 mRNA and protein expression were found to increase during mouse neuron and brain development (Alnouti et al., 2006; Hashiguchi et al., 2018; Idris et al., 2019), supporting a role for SULT4A1 in neuronal maturation. Notably, we found that SULT4A1 is not only express in cytosol, mitochondrial and microsomal fractions (Garcia et al., 2018), but is also highly expressed in synaptosomal preparation, obtained from mouse cortical neurons (Fig. 5G).

Sult4a1-KO mice present with a severe and progressive neurological phenotype, including tremor, absence seizures and ataxia, resulting in postnatal death (Garcia et al., 2018). In humans, polymorphisms in the *SULT4A1* gene have been associated with susceptibility to schizophrenia (Brennan and Condra, 2005) and several intronic polymorphism were found in patients with worse cognitive performance (Meltzer et al., 2008). Interestingly, these *SULT4A1* polymorphisms are believed to lead to a reduction of mRNA translatability (Brennan and Condra, 2005). Phelan-McDermid Syndrome (PMS) is a neurological disorder characterized by global developmental delay and autistic like behavior (Phelan and McDermid, 2012), due to deletions of the distal long arm of chromosome 22. Although it is widely recognized that deletion of *SHANK3* gene, encoding a scaffold protein of the post-synaptic density (Naisbitt et al., 1999), is the main cause of the PMS neurological phenotypes (Durand et al., 2007), the wide clinical heterogeneity among PMS patients suggests that the haploinsufficiency of other genes in the 22q13 region, beside *SHANK3*, might contribute to cognitive and speech deficits associated with PMS. Approximately 30% of patients with PMS have a deletion encompassing *SULT4A1* (Sarasua et al., 2014) and infants with *SULT4A1* deletion displayed a developmental quotient lower than patients showing two intact *SULT4A1* alleles (Zwanenburg et al., 2016). Moreover, Disciglio et al. proposed *SULT4A1* as a gene related to neurological symptoms of PMS patients (Disciglio et al., 2014). All these evidences and the high evolutionary conserved sequence in vertebrate brains (Allali-Hassani et al., 2007), strengthen the hypothesis that SULT4A1 plays a pivotal role in central nervous system development and function.

Garcia et al. showed that SULT4A1 is expressed in the neurite projections of primary cortical neurons (Garcia et al., 2018). Our morphological data show that, in cultured neurons and *in vivo*, SULT4A1 modulates neuronal branching complexity and dendritic spine density, suggesting a role of SULT4A1 in neuronal maturation and synaptic plasticity. Deficits in dendritic arborization and spine density have been characterized in Shank3 KO mice model of PMS and in mouse models of schizophrenia (Peca et al., 2011; Verpelli et al., 2011b; Glausier and Lewis, 2013; Sala and Segal,

2014; Russell et al., 2018; Gouder et al., 2019). Interestingly, we reported alteration in dendritic arborization and spine density both when we silence or overexpress SULT4A1 (Fig. 2 and 3). These observations support expression of SULT4A1 at the appropriate level as crucial to ensure proper neuronal development and function. Thus, deficits in SULT4A1 expression, and the resulting decrease in arborization and spine density, may confer developmental deficits that contribute to the presentation or severity of PMS and schizophrenia.

Electrophysiological recordings in primary neurons showed that SULT4A1 modulates NMDAR-mediated synaptic transmission. SULT4A1 silencing induced a decrease in NMDA receptor subunit GluN1 expression (Fig. 4B and Fig. 5G) and synaptic localization (Fig. 5C-G), which were associated with a significant reduction in NMDA current amplitude (Fig. 5A).

The peptidyl-prolyl *cis-trans* isomerase Pin1, highly expressed in neuronal cells, has been identified as an interactor of SULT4A1 (Smet et al., 2005; Mitchell and Minchin, 2009). However, the physiological role of this interaction is still unknown. Pin1 is a key regulator of synaptic plasticity (Antonelli et al., 2016), playing a central role in the prolyl isomerization of PSD-95. This function has been shown to negatively affect the formation of the PSD-95/NMDAR complex, that is essential for targeting NMDARs to synapses (Antonelli et al., 2016). This role is supported by the observation that neurons derived from $Pin1^{-/-}$ mice exhibit increased spine density and synaptic GluN1 and GluN2B content (Antonelli et al., 2016). In the absence of SULT4A1, we found a higher amount of Pin1 at synaptic sites associated with lower levels of GluN1 and GluN2B (Fig. 5G), as well as a decreased GluN1/PSD-95 colocalization (Fig. 5C-F). Considering the known catalytic activity of Pin1 towards PSD-95 (Antonelli et al., 2016), it is compelling to note that in co-immunoprecipitation experiments from SULT4A1-knocked down cortical neurons we detected an enhanced Pin1/PSD-95 complex formation (Fig. 5H). These results suggest that PSD-95-targeted prolyl isomerization mediated by Pin1 may be enhanced by SULT4A1 knockdown.

Notably, reduced NMDAR-mediated synaptic transmission caused by the absence of SULT4A1 expression can be rescued through pharmacological inhibition of Pin1 catalytic activity (Fig. 6A-B). In line with these results, Pin1 inhibition rescues the dendritic spines deficits in SULT4A1-knocked down neurons (Fig. 6C-D). These results support a role for SULT4A1 in the regulation of PSD-95-targeted Pin1 activity, which in turn controls GluN1 synaptic levels and the formation or stability of dendritic spines. As NMDAR function is intricately linked to synaptic maturation and activity, it is compelling to hypothesize a direct link between GluN1 synaptic levels, dendritic spine density and the well characterized behavioral deficits within SULT4A1 knockout models (Crittenden et al., 2015; Garcia et al., 2018).

In conclusion, the present study reveals a novel role for SULT4A1 in modulating neuronal morphology and synaptic activity. We propose a model in which SULT4A1 acts to sequester Pin1 from the synapse, preventing its isomerase activity towards PSD-95. As PSD-95 prolyl-isomerization has been characterized to negatively modulate the synaptic content of NMDA receptors (Antonelli et al., 2016), this sequestration facilitates the formation of PSD-95/NMDAR complexes within dendritic spines, resulting in increased NMDAR-mediated synaptic activity and dendritic spine maturation (Fig. 6E).

References

Allali-Hassani A, Pan PW, Dombrovski L, Najmanovich R, Tempel W, Dong A, Loppnau P, Martin F, Thornton J, Thonton J, Edwards AM, Bochkarev A, Plotnikov AN, Vedadi M, Arrowsmith CH (2007) Structural and chemical profiling of the human cytosolic sulfotransferases. PLoS Biol 5:e97.

Alnouti Y, Petrick JS, Klaassen CD (2006) Tissue distribution and ontogeny of organic cation transporters in mice. Drug Metab Dispos 34:477-482.

Antonelli R, De Filippo R, Middei S, Stancheva S, Pastore B, Ammassari-Teule M, Barberis A, Cherubini E, Zacchi P (2016) Pin1 Modulates the Synaptic Content of NMDA Receptors via Prolyl-Isomerization of PSD-95. J Neurosci 36:5437-5447.

Blanchard RL, Freimuth RR, Buck J, Weinshilboum RM, Coughtrie MW (2004) A proposed nomenclature system for the cytosolic sulfotransferase (SULT) superfamily. Pharmacogenetics 14:199-211.

Borroni B, Stanic J, Verpelli C, Mellone M, Bonomi E, Alberici A, Bernasconi P, Culotta L, Zianni E, Archetti S, Manes M, Gazzina S, Ghidoni R, Benussi L, Stuani C, Di Luca M, Sala C, Buratti E, Padovani A, Gardoni F (2017) Anti-AMPA GluA3 antibodies in Frontotemporal dementia: a new molecular target. Sci Rep 7:6723.

Brennan MD, Condra J (2005) Transmission disequilibrium suggests a role for the sulfotransferase-4A1 gene in schizophrenia. Am J Med Genet B Neuropsychiatr Genet 139B:69-72.

Chen Y, Stevens B, Chang J, Milbrandt J, Barres BA, Hell JW (2008) NS21: re-defined and modified supplement B27 for neuronal cultures. J Neurosci Methods 171:239-247.

Crittenden F, Thomas HR, Parant JM, Falany CN (2015) Activity Suppression Behavior Phenotype in SULT4A1 Frameshift Mutant Zebrafish. Drug Metab Dispos 43:1037-1044.

Disciglio V et al. (2014) Interstitial 22q13 deletions not involving SHANK3 gene: a new contiguous gene syndrome. Am J Med Genet A 164A:1666-1676.

Durand CM et al. (2007) Mutations in the gene encoding the synaptic scaffolding protein SHANK3 are associated with autism spectrum disorders. Nat Genet 39:25-27.

Falany CN, Xie X, Wang J, Ferrer J, Falany JL (2000) Molecular cloning and expression of novel sulphotransferase-like cDNAs from human and rat brain. Biochem J 346 Pt 3:857-864.

Garcia PL, Hossain MI, Andrabi SA, Falany CN (2018) Generation and Characterization of SULT4A1 Mutant Mouse Models. Drug Metab Dispos 46:41-45.

Glausier JR, Lewis DA (2013) Dendritic spine pathology in schizophrenia. Neuroscience 251:90-107.

Gouder L, Vitrac A, Goubran-Botros H, Danckaert A, Tinevez JY, Andre-Leroux G, Atanasova E, Lemiere N, Biton A, Leblond CS, Poulet A, Boland A, Deleuze JF, Benchoua A, Delorme R, Bourgeron T, Cloez-Tayarani I (2019) Altered spinogenesis in iPSC-derived cortical neurons from patients with autism carrying de novo SHANK3 mutations. Sci Rep 9:94.

Hashiguchi T, Shindo S, Chen SH, Hong JS, Negishi M (2018) Sulfotransferase 4A1 Increases Its Expression in Mouse Neurons as They Mature. Drug Metab Dispos 46:860-864.

618 Idris M, Butcher NJ, Minchin RF (2019) The MBNL/CELF Splicing Factors Regulate Cytosolic
619 Sulfotransferase 4A1 protein expression During Cell Differentiation. Drug Metab Dispos.
620 Liyou NE, Buller KM, Tresillian MJ, Elvin CM, Scott HL, Dodd PR, Tannenberg AE, McManus ME
621 (2003) Localization of a brain sulfotransferase, SULT4A1, in the human and rat brain: an
622 immunohistochemical study. J Histochem Cytochem 51:1655-1664.
623 Lois C, Hong EJ, Pease S, Brown EJ, Baltimore D (2002) Germline transmission and tissue-specific
624 expression of transgenes delivered by lentiviral vectors. Science 295:868-872.
625 Meltzer HY, Brennan MD, Woodward ND, Jayathilake K (2008) Association of Sult4A1 SNPs with
626 psychopathology and cognition in patients with schizophrenia or schizoaffective disorder.
627 Schizophr Res 106:258-264.
628 Minchin RF, Lewis A, Mitchell D, Kadlubar FF, McManus ME (2008) Sulfotransferase 4A1. Int J
629 Biochem Cell Biol 40:2686-2691.
630 Mitchell DJ, Minchin RF (2009) Cytosolic Aryl sulfotransferase 4A1 interacts with the peptidyl
631 prolyl cis-trans isomerase Pin1. Mol Pharmacol 76:388-395.
632 Mitz AR, Philyaw TJ, Boccuto L, Shcheglovitov A, Sarasua SM, Kaufmann WE, Thurm A (2018)
633 Identification of 22q13 genes most likely to contribute to Phelan McDermid syndrome. Eur J Hum
634 Genet 26:293-302.
635 Naisbitt S, Kim E, Tu JC, Xiao B, Sala C, Valtschanoff J, Weinberg RJ, Worley PF, Sheng M (1999)
636 Shank, a novel family of postsynaptic density proteins that binds to the NMDA receptor/PSD-
637 95/GKAP complex and cortactin. Neuron 23:569-582.
638 Naldini L, Blomer U, Gallay P, Ory D, Mulligan R, Gage FH, Verma IM, Trono D (1996) In vivo gene
639 delivery and stable transduction of nondividing cells by a lentiviral vector. Science 272:263-267.
640 Negishi M, Pedersen LG, Petrotchenko E, Shevtsov S, Gorokhov A, Kakuta Y, Pedersen LC (2001)
641 Structure and function of sulfotransferases. Arch Biochem Biophys 390:149-157.
642 Osborn M, Weber K (1982) Immunofluorescence and immunocytochemical procedures with
643 affinity purified antibodies: tubulin-containing structures. Methods Cell Biol 24:97-132.
644 Peca J, Feliciano C, Ting JT, Wang W, Wells MF, Venkatraman TN, Lascola CD, Fu Z, Feng G (2011)
645 Shank3 mutant mice display autistic-like behaviours and striatal dysfunction. Nature 472:437-442.
646 Phelan K, McDermid HE (2012) The 22q13.3 Deletion Syndrome (Phelan-McDermid Syndrome).
647 Mol Syndromol 2:186-201.
648 Ramsey TL, Meltzer HY, Brock GN, Mehrotra B, Jayathilake K, Bobo WV, Brennan MD (2011)
649 Evidence for a SULT4A1 haplotype correlating with baseline psychopathology and atypical
650 antipsychotic response. Pharmacogenomics 12:471-480.
651 Ranganathan R, Lu KP, Hunter T, Noel JP (1997) Structural and functional analysis of the mitotic
652 rotamase Pin1 suggests substrate recognition is phosphorylation dependent. Cell 89:875-886.
653 Russell TA, Grubisha MJ, Remmers CL, Kang SK, Forrest MP, Smith KR, Kopeikina KJ, Gao R, Sweet
654 RA, Penzes P (2018) A Schizophrenia-Linked KALRN Coding Variant Alters Neuron Morphology,
655 Protein Function, and Transcript Stability. Biol Psychiatry 83:499-508.
656 Sala C, Segal M (2014) Dendritic spines: the locus of structural and functional plasticity. Physiol Rev
657 94:141-188.
658 Sarasua SM, Dwivedi A, Boccuto L, Chen CF, Sharp JL, Rollins JD, Collins JS, Rogers RC, Phelan K,
659 DuPont BR (2014) 22q13.2q13.32 genomic regions associated with severity of speech delay,
660 developmental delay, and physical features in Phelan-McDermid syndrome. Genet Med 16:318-
661 328.
662 Sessa A, Mao CA, Hadjantonakis AK, Klein WH, Broccoli V (2008) Tbr2 directs conversion of radial
663 glia into basal precursors and guides neuronal amplification by indirect neurogenesis in the
664 developing neocortex. Neuron 60:56-69.

Shen M, Stukenberg PT, Kirschner MW, Lu KP (1998) The essential mitotic peptidyl-prolyl isomerase Pin1 binds and regulates mitosis-specific phosphoproteins. Genes Dev 12:706-720.
Sidharthan NP, Butcher NJ, Mitchell DJ, Minchin RF (2014) Expression of the orphan cytosolic sulfotransferase SULT4A1 and its major splice variant in human tissues and cells: dimerization, degradation and polyubiquitination. PLoS One 9:e101520.
Smet C, Wieruszeski JM, Buee L, Landrieu I, Lippens G (2005) Regulation of Pin1 peptidyl-prolyl cis/trans isomerase activity by its WW binding module on a multi-phosphorylated peptide of Tau protein. FEBS Lett 579:4159-4164.
Tatara Y, Terakawa T, Uchida T (2010) Identification of Pin1-binding phosphorylated proteins in the mouse brain. Biosci Biotechnol Biochem 74:2480-2483.
Verpelli C, Piccoli G, Zanchi A, Gardoni F, Huang K, Brambilla D, Di Luca M, Battaglioli E, Sala C (2010) Synaptic Activity Controls Dendritic Spine Morphology by Modulating eEF2-Dependent BDNF Synthesis. Journal of Neuroscience 30:5830-5842.
Verpelli C, Dvoretskova E, Vicidomini C, Rossi F, Chiappalone M, Schoen M, Di Stefano B, Mantegazza R, Broccoli V, Böckers TM, Dityatev A, Sala C (2011a) Importance of Shank3 protein in regulating metabotropic glutamate receptor 5 (mGluR5) expression and signaling at synapses. J Biol Chem 286:34839-34850.
Verpelli C, Dvoretskova E, Vicidomini C, Rossi F, Chiappalone M, Schoen M, Di Stefano B, Mantegazza R, Broccoli V, Bockers TM, Dityatev A, Sala C (2011b) Importance of Shank3 protein in regulating metabotropic glutamate receptor 5 (mGluR5) expression and signaling at synapses. J Biol Chem 286:34839-34850.
Vicidomini C, Ponzoni L, Lim D, Schmeisser MJ, Reim D, Morello N, Orellana D, Tozzi A, Durante V, Scalmani P, Mantegazza M, Genazzani AA, Giustetto M, Sala M, Calabresi P, Boeckers TM, Sala C, Verpelli C (2017) Pharmacological enhancement of mGlu5 receptors rescues behavioral deficits in SHANK3 knock-out mice. Mol Psychiatry 22:689-702.
Wiznerowicz M, Trono D (2003) Conditional suppression of cellular genes: lentivirus vector-mediated drug-inducible RNA interference. J Virol 77:8957-8961.
Ziats CA, Grosvenor LP, Sarasua SM, Thurm AE, Swedo SE, Mahfouz A, Rennert OM, Ziats MN (2019) Functional genomics analysis of Phelan-McDermid syndrome 22q13 region during human neurodevelopment. PLoS One 14:e0213921.
Zwanenburg RJ, Bocca G, Ruiter SA, Dillingh JH, Flapper BC, van den Heuvel ER, van Ravenswaaij-Arts CM (2016) Is there an effect of intranasal insulin on development and behaviour in Phelan-McDermid syndrome? A randomized, double-blind, placebo-controlled trial. Eur J Hum Genet 24:1696-1701.

Figure legends

Figure 1 | Physiological expression of SULT4A1 protein during neuronal development. A Representative western blots of total cell lysates derived from rat cortical neurons at different days in-vitro (n=4 independent cultures for all conditions; One-way ANOVA test, $P<0.0001$; Tukey's *post-hoc* test, ** P=0.0011, *** P=0.0001, **** P<0.0001). **B** Biochemical analysis of total brain lysates derived from wild type male mice at different post-natal days (n=3 animals for all conditions). **C** Representative western blots of protein lysates from hippocampus (H), striatum (S), cerebral cortex (Cx) and cerebellum (Cb) derived from adult (P60) wild type mice (n=4 animals for all conditions; Kruskal-Wallis test, $P<0.0001$; Dunn's *post-hoc* test, * P=0.0451; ** P=0.0065). **D** Area-specific expression of SULT4A1 was also compared between adult male (M) and female (F) mice (n=3 animals for all conditions; Two-way ANOVA, $P=0.8362$; Sidak's *post-hoc* test)**. E** Representative immunocytochemical staining for SULT4A1 (green), βIII-Tubulin (red) and DAPI (blue), in rat cortical neurons at day-in-vitro (DIV) 1, 7 and 14. Scale bar = 50µm. **F** Left: representative immunocytochemical staining of Oct4 (green), Sox2 (red) and DAPI (blue) of induced pluripotent stem cells (iPSCs) obtained from healthy control individuals. Center: iPSC-derived neural stem cells (NSCs) stained for Nestin (green), Sox2 (red) and DAPI (blue). Right: representative immunostaining for MAP2 (green) and DAPI (blue) of NSC-derived neurons after 40 days of differentiation. Scale bar = 50µm. **G** Representative immunoblots of total cell lysates obtained from human neurons, sampled during differentiation from day 0 (NSC stage) until day 40 (mature neuron stage) (n=3 independent cultures for all conditions; One-way ANOVA test, $P<0.0001$; Tukey's *post-hoc* test, 0 vs 30: P<0.0001, 0 vs 40: P<0.0001, 10 vs 20: P=0.0371, 10 vs 30: P<0.0001, 10 vs 40: P<0.0001, 20 vs 30: P=0.0003, 20 vs 40: P<0.0001, 30 vs 40: P=0.0411). Data represent Mean ± SEM.

Figure 2 | *Sult4a1* silencing reduces neuronal branching and dendritic spine density. A Representative immunofluorescence images and relative traces of rat cortical neurons transfected with the scrambled shRNA (shCtrl), the *Sult4a1*-specific shRNA (sh*Sult4a1*) or sh*Sult4a1* together with the resistant construct (*Sult4a1*r). Neurons were stained for SULT4A1 (red) to assess protein expression. Scale bar= 100 µm. **B** Results of Sholl analysis and quantification of the number of intersections, plotted against the distance from the soma (shCtrl n=13 individual neurons, sh*Sult4a1* n=15 individual neurons, *Sult4a1*r n=19 individual neurons; Two-way ANOVA, $P<0.0001$; Tukey's *post-hoc* test, * sh*Sult4a1* vs shCtrl, # sh*Sult4a1* vs *Sult4a1*r; 30µm: ****P<0.0001, ## P<0.0001; 40µm: ****P<0.0001, ####P<0.0001; 50µm: ****P<0.0001, ###P=0.0001; 60µm:

741 ***P=0.0007). **C** Quantification of total dendrites length (shCtrl n=10 individual neurons,
742 sh*Sult4a1* n=13 individual neurons, *Sult4a1*r n=13 individual neurons; One-way ANOVA,
743 *P*<0.0001, Tukey's *post-hoc* test, shCtrl vs sh*Sult4a1:* P=0.0001, sh*Sult4a1* vs *Sult4a1r*: P=0.0001,
744 ns= not significant). **D-E** Quantification of the number of primary (D) and secondary (E) dendrites
745 (shCtrl n=21 individual neurons, sh*Sult4a1* n=18 individual neurons, *Sult4a1*r n=20 individual
746 neurons; (D): One-way ANOVA, *P*<0.0001, Tukey's *post-hoc* test, shCtrl vs sh*Sult4a1:* P=0.0002,
747 sh*Sult4a1* vs *Sult4a1r*: P=0.0002, ns= not significant; (E): One-way ANOVA, *P*<0.0001, Tukey's
748 *post-hoc* test, shCtrl vs sh*Sult4a1:* P<0.0001, sh*Sult4a1* vs *Sult4a1r*: P=0.0079, ns= not significant).
749 **F** Representative immunofluorescence images showing dendritic spines of rat cortical neurons
750 transfected with shCtrl, sh*Sult4a1* or sh*Sult4a1* together with the resistant plasmid. Neurons were
751 stained for SULT4A1 (red) to assess protein expression. Scale bar= 10 µm. **G-I** Quantification of
752 dendritic spines length (G), width (H) and number of spines per 10 µm of dendrite (I) (shCtrl n=10
753 individual dendrites, sh*Sult4a1* n=10 individual dendrites, *Sult4a1*r n=14 individual dendrites;
754 Kruskal-Wallis test, *P*=0.6092 for (G), *P*=0.8472 for (H), *P*=0.0081 for (I); (I): Dunn's *post-hoc*
755 test, shCtrl vs sh*Sult4a1:* P=0.0105, sh*Sult4a1* vs *Sult4a1r*: P=0.0417, ns= not significant). **J**
756 Quantification of filopodia, long thin and mushroom spines distribution. **K** Representative
757 immunohistochemistry images from brain slices obtained from 30-day-old in utero electroporated
758 mice, showing cortical neurons expressing shCtrl or shSult4a1 and their relative traces. Scale bar=
759 100 µm. **L** Results of Sholl analysis and quantification of the number of intersections, plotted
760 against the distance from the soma (shCtrl n=10 individual neurons, shSult4a1 n=13 individual
761 neurons; Two-way ANOVA, P=0.0629; Sidak's post-hoc test, 60µm: *P=0.0162; 70µm:
762 ****P<0.0001). **M** Quantification of total dendrites length (shCtrl n=10 individual neurons,
763 sh*Sult4a1* n=13 individual neurons, Unpaired t test *** P=0.0002). **N** Representative
764 immunofluorescence images showing dendritic spines of shCtrl- or sh*Sult4a1*-expressing cortical
765 neurons from 30-day-old in utero electroporated mice. Scale bar= 10 µm. **O-Q** Quantification of
766 dendritic spines length (O), width (P) and number of spines per 10 µm of dendrite (Q) (shCtrl n= 12
767 individual dendrites, shSult4a1 n= 9 individual dendrites; Unpaired t test P=0.0490). **R**
768 Quantification of thin, stubby and mushroom spines distribution. Data represent Mean ± SEM.
769
770 **Figure 3 | *Sult4a1* overexpression impairs dendritic arborization and spines.** **A** Representative
771 immunofluorescence images and relative traces of rat cortical neurons transfected with pLVTHM
772 alone (GFP) or together with pFlag-SULT4A1 (overexpression). Neurons were stained for
773 SULT4A1 (red) to assess protein (over)expression. Scale bar= 100 µm. **B** Results of Sholl analysis
774 and quantification of the number of intersections, plotted against the distance from the soma (GFP

n=21 individual neurons, Overexpression n=15 individual neurons; Two-way ANOVA, $P<0.0001$; Sidak's *post-hoc* test, 10µm: *P=0.0126; 20µm: *P=0.0444). **C-D** Quantification of the number of primary (C) and secondary (D) dendrites (GFP n=20 individual neurons, Overexpression (OV) n=21 individual neurons; for (C) Mann-Whitney test, $P=0.3511$; for (D) Unpaired *t* test, $P=0.2496$). **E** Quantification of total dendrites length (GFP n=20 individual neurons, Overexpression (OV) n=21 individual neurons; Unpaired *t* test, $P=0.2387$). **F** Representative immunofluorescence images showing dendritic spines of rat cortical neurons transfected with pLVTHM alone (GFP) or together with pFlag-SULT4A1 (OV). Neurons were stained for SULT4A1 (red) to assess protein (over)expression. Scale bar= 10 µm. **G-I** Quantification of dendritic spines length (G), width (H) and number of spines per 10 µm of dendrite (I) (GFP n=15 individual dendrites, OV n=23 individual dendrites; Unpaired *t* test (G):**P=0.0126; (I):):*P=0.0303). **J** Quantification of filopodia, long thin and mushroom spines distribution. Data represent Mean ± SEM.

Figure 4 | *Sult4a1* knockdown alters synaptic transmission. A Representative immunoblots of total protein lysates derived from day-in-vitro 14 rat cortical neurons transduced with a lentivirus expressing shCtrl or sh*Sult4a1*. Both conditions were compared with not infected condition (Ni) so to verify whether the infection itself could cause any alteration of Sult4a1 protein expression. Sult4a1 protein levels were normalized against the level of the not infected neurons (Ni n=7 independent cultures, shCtrl n=4 independent cultures, sh*Sult4a1* n=7 independent cultures; One-sample *t* test, Ni vs sh*Sult4a1:*****P<0.0001, shCtrl vs sh*Sult4a1:*****P<0.0001, ns= not significant). **B** Representative western blots of total lysates from shCtrl- or sh*Sult4a1*-transduced cortical neurons. Protein levels were normalized against the level of the shCtrl-transduced neurons. (shCtrl n≥3 independent cultures, sh*Sult4a1* n≥3 independent cultures; One-sample *t* test, GAD65:*P=0.0396, GluN1:*P=0.0186). **C** Upper panels: representative spontaneous excitatory postsynaptic currents (sEPSCs) recorded from shCtrl- (blue) or sh*Sult4a1*- (red) transfected neurons. Middle panels: left, plot of cumulative probability of sEPSC frequencies (shCtrl n=5 individual neurons, sh*Sult4a1* n=5 individual neurons; Kolmogorov-Smirnov test, $P=4\times10^{-18}$); right, mean instantaneous frequencies plot (shCtrl n=5 individual neurons, sh*Sult4a1* n=5 individual neurons; Mann-Whitney test, * $P<0.05$; data are shown as Mean ± SEM). Bottom panels: left, plot of cumulative probability of sEPSC amplitudes (Kolmogorov-Smirnov test, $P=10^{-11}$); right, plot of mean sEPSC amplitudes (shCtrl n=5 individual neurons, sh*Sult4a1* n=5 individual neurons; Mann-Whitney test, $P=10^{-12}$; data are shown as Mean ± SEM). **D** Upper panels: representative spontaneous inhibitory postsynaptic currents (sIPSCs) recorded from shCtrl- (blue) or sh*Sult4a1*- (red) transfected neurons. Middle panels: left, plot of cumulative probability of sIPSC frequencies

(shCtrl n=5 individual neurons, sh*Sult4a1* n=6 individual neurons; Kolmogorov-Smirnov test, $P=5x10^{-8}$): right: plot of mean instantaneous frequencies (shCtrl n=5 individual neurons, sh*Sult4a1* n=6 individual neurons; Mann-Whitney test; data are shown as Mean ± SEM). Bottom panels: left, plot of cumulative probability of sIPSC amplitudes (Kolmogorov-Smirnov test, $P=10^{-12}$); right, plot of mean sIPSC amplitudes (shCtrl n=5 individual neurons, sh*Sult4a1* n=5 individual neurons; Mann-Whitney test, $P=10^{-8}$; data are shown as Mean ± SEM).

Figure 5 | SULT4A1 interaction with Pin1 and its role in excitatory synapses. A Left: representative NMDA-mediated current (I_{NMDA}) traces elicited by the perfusion of 100 µM NMDA from neurons transfected with shCtrl (blue), sh*Sult4a1* (red) or sh*Sult4a1* together with the resistant plasmid *Sult4a1r* (orange). Right: analysis of mean peak I_{NMDA} current densities in neurons transfected with shCtrl, sh*Sult4a1* or sh*Sult4a1* together with the resistant plasmid *Sult4a1r* (shCtrl n=30 individual neurons, sh*Sult4a1* n=34 individual neurons; *Sult4a1r* n=10; One-way ANOVA, P=0.0028, Tukey's post-hoc test, shCtrl vs sh*Sult4a1*: P=0.0048, sh*Sult4a1* vs *Sult4a1r*: P=0.0423, ns= not significant). **B** Left: representative AMPA-mediated current (I_{AMPA}) traces elicited by the perfusion of 100 µM AMPA from neurons transfected with shCtrl (blue), sh*Sult4a1* (red) or sh*Sult4a1* together with the resistant plasmid *Sult4a1r* (orange). Right: analysis of mean peak I_{AMPA} current densities in neurons transfected with shCtrl, sh*Sult4a1* or sh*Sult4a1* together with the resistant plasmid *Sult4a1r* (shCtrl n=11 individual neurons, sh*Sult4a1* n=8 individual neurons; *Sult4a1r* n=7 individual neurons; One-way ANOVA, P=0.2133). **C** Representative immunofluorescence images showing dendritic spines of rat cortical neurons transfected with shCtrl or sh*Sult4a1*. Neurons were stained for PSD-95 (blue) and GluN1 (red). Scale bar= 10 µm. **D-E** Quantification of the number of PSD-95 (D) and GluN1 (E) clusters per 10 µm of dendrite (shCtrl n=11 individual dendrites, sh*Sult4a1* n=11 individual dendrites; Unpaired *t* test, (E): P=0.0003). **F** Quantification of GluN1 and PSD-95 clusters colocalization (shCtrl n=11 individual dendrites, sh*Sult4a1* n=11 individual dendrites; Unpaired *t* test, *** P=0.0004). **G** Representative western blots of synaptosomal fractions obtained from cortical neurons transduced with shCtrl or sh*Sult4a1*. Protein levels were normalized against the levels of the shCtrl-transduced neurons (shCtrl n≥3 independent cultures, sh*Sult4a1* n≥3 independent cultures; One-sample *t* test, SULT4A1: P<0.0001, GluN1: P=0.0032, Pin1: P=0.0206). **H** Left: representative images of immunoprecipitation (IP) assay performed on synaptosomal fractions derived from neurons transduced with shCtrl or sh*Sult4a1*. Proteins were precipitated using mouse anti-Pin1 or mouse IgG antibodies and nitrocellulose membranes were probed with anti-Pin1, anti-SULT4A1 and anti-PSD-95 antibodies (WB). Right: histogram showing the ratio between PSD-95 and Pin1 signals (PSD-95/Pin1) (shCtrl

n=4 independent experiments, sh*Sult4a1* n=4 independent experiments; Unpaired *t* test, P=0.0464). Data represent Mean ± SEM.

Figure 6 | Rescue of sh*Sult4a1*-dependent phenotypes via Pin1 pharmacological inhibition. A Left: representative NMDA-mediated current (I_{NMDA}) traces from shCtrl- (blue) and sh*Sult4a1*- (red) transfected neurons, treated for 48h with 2.5 µM PiB or vehicle. Right: analysis of mean peak I_{NMDA} current densities (shCtrl + vehicle n=12 individual neurons, shCtrl + PiB n=16 individual neurons, sh*Sult4a1* + vehicle n=6 individual neurons, sh*Sult4a1* + PiB n=16 individual neurons; One-way ANOVA, *P*=0.0082; Tukey's *post-hoc* test, shCtrl vehicle vs sh*Sult4a1* vehicle: P=0.0146, sh*Sult4a1* vehicle vs sh*Sult4a1* PiB: P=0.0186). **B** Left: representative NMDA-mediated current (I_{NMDA}) traces from shCtrl- (blue) and sh*Sult4a1*- (red) transfected neurons, treated for 48h with 4 µM DTM or vehicle. Right: analysis of mean peak I_{NMDA} current densities (shCtrl + vehicle n= 16 individual neurons, shCtrl + DTM n= 7 individual neurons, sh*Sult4a1* + vehicle n= 21 individual neurons, sh*Sult4a1* + DTM n= 10 individual neurons; One-way ANOVA, P=0,0008, Tukey's *post-hoc* test, shCtrl+vehicle vs sh*Sult4a1*+vehicle: P=0.0455, sh*Sult4a1*+vehicle vs sh*Sult4a1*+DTM: P=0.0006). **C** Left: representative immunofluorescence images showing dendritic spines of rat cortical neurons transfected with shCtrl or sh*Sult4a1* and treated for 48h with 2.5 µM PiB, a pharmacological inhibitor of Pin1 catalytic activity, or vehicle (DMSO). Scale bar=10µm. Right: quantification of the number of dendritic spines per 10 µm of dendrite (shCtrl + vehicle n=19 individual dendrites, shCtrl + PiB n=16 individual dendrites, sh*Sult4a1* + vehicle n=19 individual dendrites, sh*Sult4a1* + PiB n=17 individual dendrites; One-way ANOVA, *P*=0.0003; Tukey's *post-hoc* test, shCtrl+vehicle vs sh*Sult4a1*+vehicle: P=0.0096, shCtrl+PiB vs sh*Sult4a1* vehicle: P=0.0005, sh*Sult4a1*+vehicle vs sh*Sult4a1*+PiB: P=0.0044). **D** Left: representative immunofluorescence images showing dendritic spines of rat cortical neurons transfected with shCtrl or sh*Sult4a1* and treated at DIV12 for 48h with 4 µM DTM, a pharmacological inhibitor of Pin1 catalytic activity, or vehicle (DMSO); scale bar=10 µm. Right: quantification of the number of dendritic spines per 10 µm of dendrite (shCtrl + vehicle n=10 individual dendrites, shCtrl + DTM n=10 individual dendrites, sh*Sult4a1* + vehicle n=11 individual dendrites, sh*Sult4a1* + DTM n=10 individual dendrites; Kruskal-Wallis test P=0.0006; Dunn's *post-hoc* test, shCtrl+vehicle vs sh*Sult4a1*+vehicle: P=0.0301, shCtrl+DTM vs sh*Sult4a1* vehicle: P=0.0012, sh*Sult4a1*+vehicle vs sh*Sult4a1*+DTM: P=0.0005). **E** Cartoon showing the hypothesized mechanism. SULT4A1 interacts with Pin1 promoting the formation of the PSD-95/NMDAR complex in excitatory synapses. In absence of SULT4A1, Pin1 is free to interact with PSD-95, reducing NMDAR expression in synapses. Data represents Mean ± SEM.

Figure 7 | Pin1 pharmacological inhibition does not rescue dendritic arborization after sh*Sult4a1* knockdown. **A** Representative immunofluorescence images and relative traces of rat cortical neurons transfected with shCtrl or sh*Sult4a1* and treated every other day with 1 μM PiB or vehicle, starting at DIV7. Scale bar= 100 μm. **B-C** Results of Sholl analysis and quantification of the number of intersections, plotted against the distance from the soma. shCtrl (B) and sh*Sult4a1* (C) conditions are displayed separately to clearly illustrate the effect of PiB treatment (B: shCtrl + vehicle n= 10 individual neurons, shCtrl + PiB n= 11 individual neurons; Two-way RM ANOVA, *P*=0.9999; Sidak's *post-hoc* test) (C: sh*Sult4a1* + vehicle n= 5 individual neurons, sh*Sult4a1* + PiB n= 11 individual neurons; Two-way RM ANOVA, *P*=0.9671; Sidak's *post-hoc* test). **D** Representative immunofluorescence images and relative traces of rat cortical neurons transfected with shCtrl or sh*Sult4a1* and treated every other day with 4 μM DTM or vehicle, starting at DIV7. Scale bar= 100 μm. **E-F** Results of Sholl analysis and quantification of the number of intersections, plotted against the distance from the soma. shCtrl (E) and sh*Sult4a1* (F) conditions are displayed separately to clearly illustrate the effect of DTM treatment (E: shCtrl + vehicle n= 9 individual neurons, shCtrl + DTM n= 9 individual neurons; Two-way RM ANOVA, *P*=0.9021; Sidak's *post-hoc* test) (F: sh*Sult4a1* + vehicle n= 6 individual neurons, sh*Sult4a1* + DTM n= 6 individual neurons; Two-way RM ANOVA, *P*=0.0886; Sidak's *post-hoc* test). Data represents Mean ± SEM.

Extended data legend

Extended data Figure 2-1 | Sult4a1-specific shRNA validation. A Western blot from HEK293T cells transfected with a plasmid expressing pLVTHM (Ctrl) or one of the two shRNA specific for Sult4a1 (shRNA #1 or shRNA #2). All constructs express GFP. Sult4a1 protein level is graphed as percentage compared to the control condition (Ctrl) (n=3 independent experiments for all conditions; One-sample t test, Ctrl vs shRNA#1: P=0.0002; Ctrl vs shRNA#2: P=0.0003). **B** Western blot from HEK293T cells transfected with a plasmid expressing the scrambled form of the shRNA (shCtrl), the shRNA #1 (now indicated as shSult4a1) alone or together with the construct resistant to interference by shSult4a1 (Sult4a1r). Both shCtrl and shSult4a1 constructs also express GFP. Sult4a1 protein level is graphed as percentage compared to the control condition (shCtrl) (n=3 independent experiments for all conditions; One-sample t test, shCtrl vs shSult4a1: P=0.0024; shCtrl vs shSult4a1+Sult4a1r: P=0.0006). Data represent Mean ± SEM.

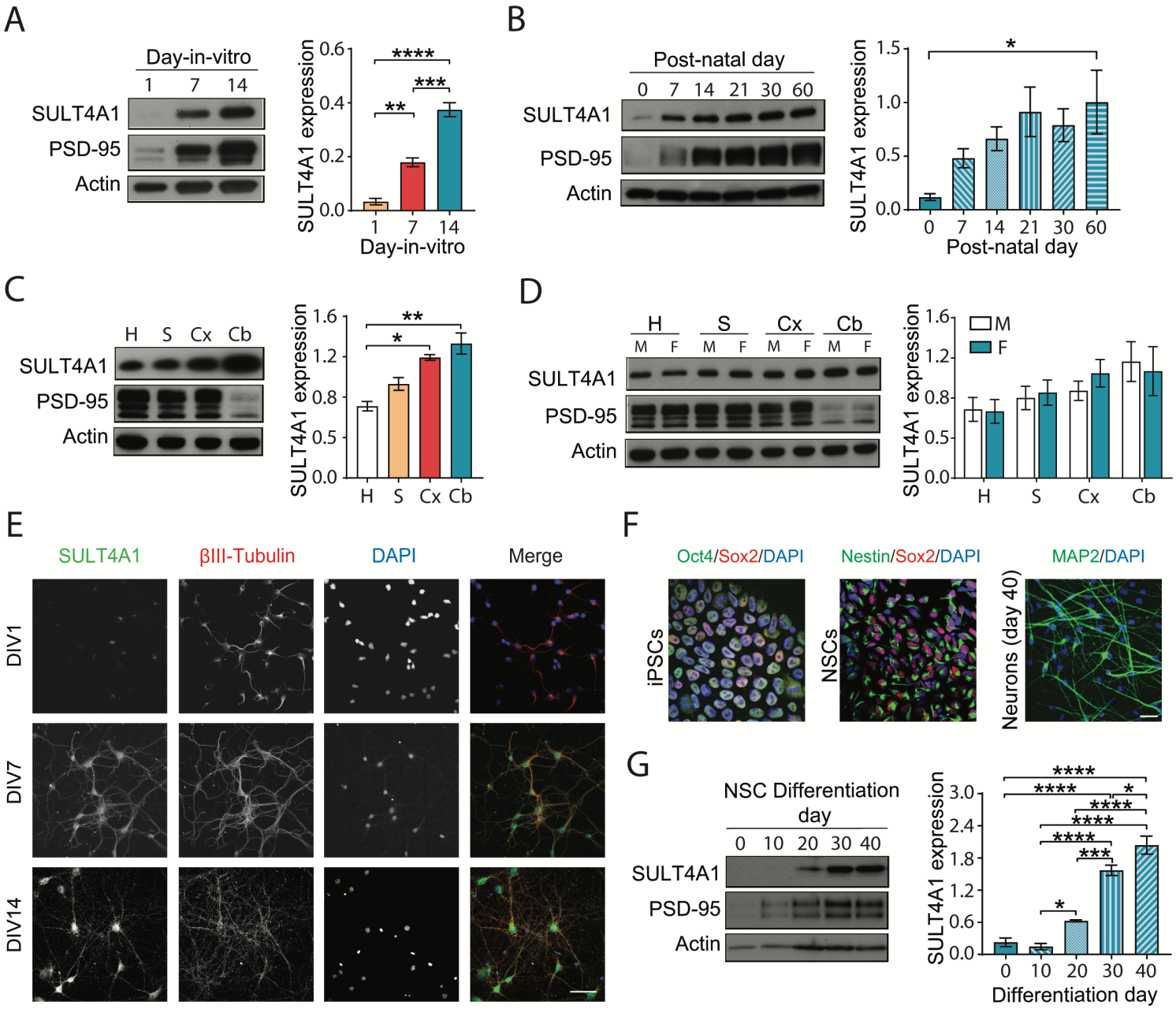
A
Day-in-vitro
1 7 14
SULT4A1
PSD-95
Actin
SULT4A1 expression
0.6
0.4
0.2
0.0
****
***
**
1 7 14
Day-in-vitro
B
Post-natal day
0 7 14 21 30 60
SULT4A1
PSD-95
Actin
SULT4A1 expression
1.5
1.0
0.5
0.0
*
0 7 14 21 30 60
Post-natal day
C
H S Cx Cb
SULT4A1
PSD-95
Actin
SULT4A1 expression
1.6
1.2
0.8
0.5
0.0
**
*
H S Cx Cb
D
H S Cx Cb
M F M F M F M F
SULT4A1
PSD-95
Actin
SULT4A1 expression
1.6
1.2
0.8
0.5
0.0
M
F
H S Cx Cb
E
SULT4A1
βIII-Tubulin
DAPI
Merge
DIV1
DIV7
DIV14
F
Oct4/Sox2/DAPI
Nestin/Sox2/DAPI
MAP2/DAPI
iPSCs
NSCs
Neurons (day 40)
G
NSC Differentiation day
0 10 20 30 40
SULT4A1
PSD-95
Actin
SULT4A1 expression
3.0
2.4
1.8
1.2
0.6
0.0
****
****
*
****
****
****
***
*
0 10 20 30 40
Differentiation day

Figure 1

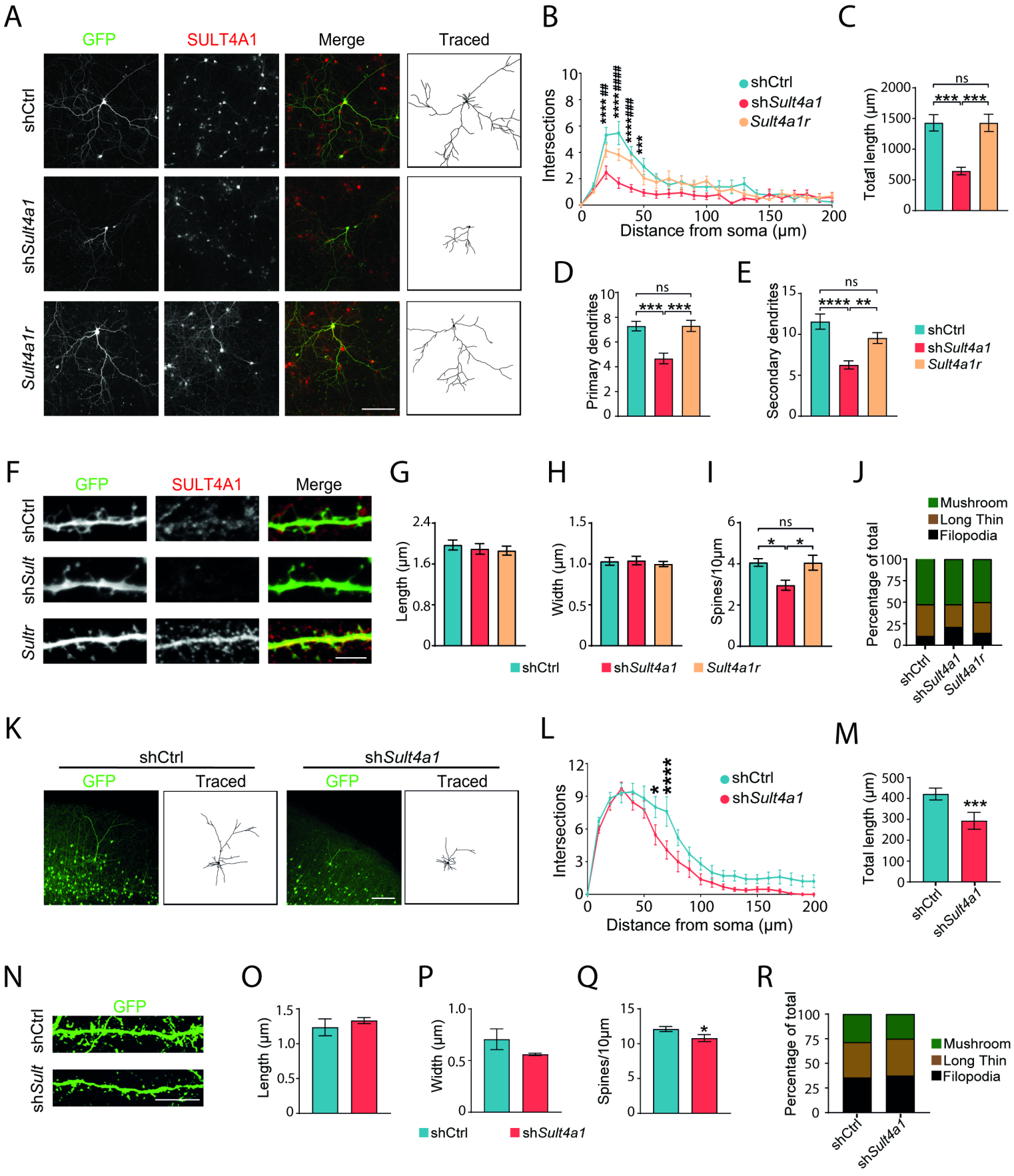
A
GFP
SULT4A1
Merge
Traced
shCtrl
shSult4a1
Sult4a1r
B
Intersections
Distance from soma (μm)
shCtrl
shSult4a1
Sult4a1r
C
Total length (μm)
ns
D
Primary dendrites
E
Secondary dendrites
F
GFP
SULT4A1
Merge
shCtrl
shSult
Sultr
G
Length (μm)
H
Width (μm)
I
Spines/10μm
J
Mushroom
Long Thin
Filopodia
Percentage of total
K
shCtrl
shSult4a1
GFP
Traced
L
Intersections
Distance from soma (μm)
M
Total length (μm)
N
GFP
shCtrl
shSult
O
Length (μm)
P
Width (μm)
Q
Spines/10μm
R
Mushroom
Long Thin
Filopodia
Percentage of total

Figure 2

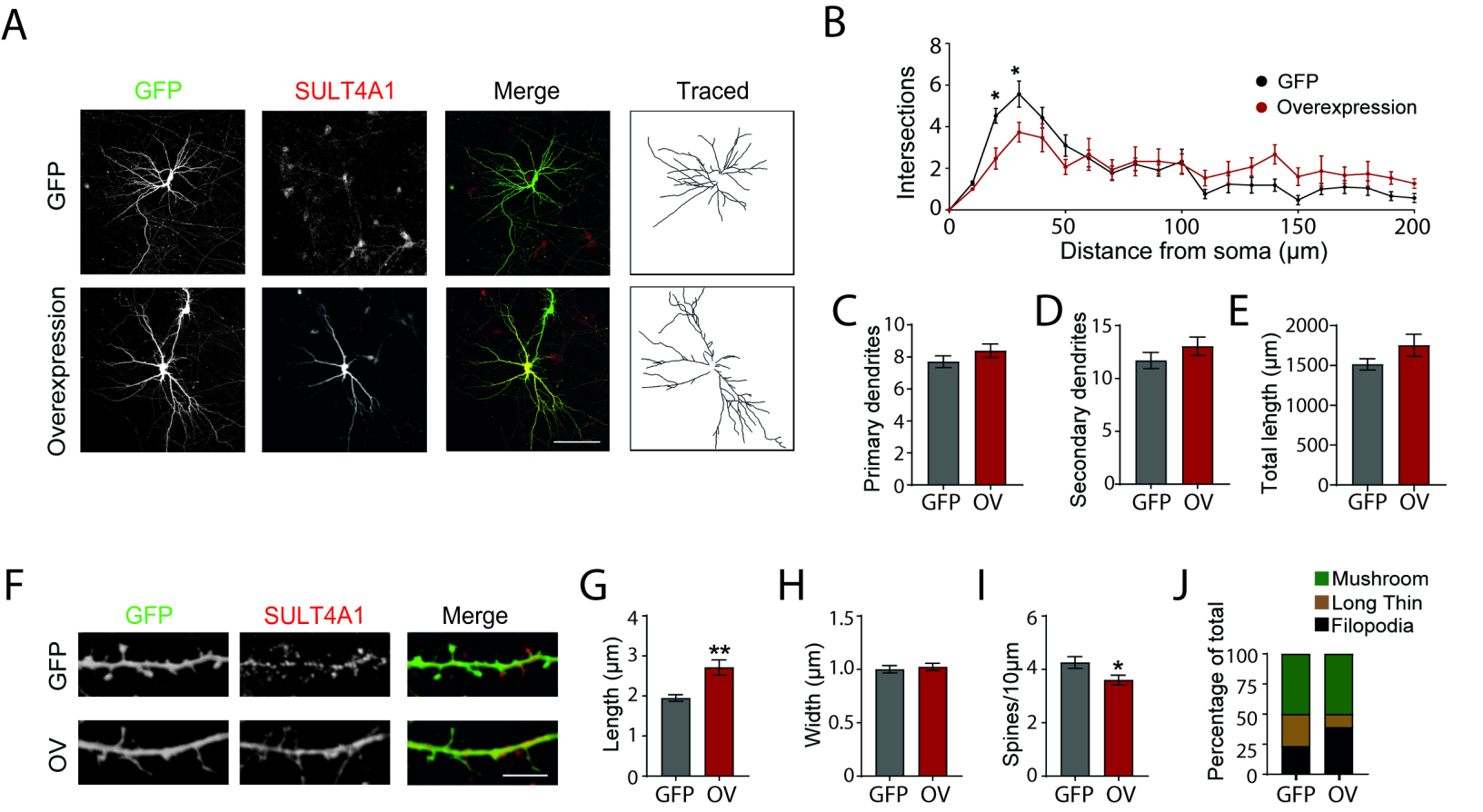
A
GFP
SULT4A1
Merge
Traced
GFP
Overexpression
B
Intersections
Distance from soma (μm)
GFP
Overexpression
C
Primary dendrites
D
Secondary dendrites
E
Total length (μm)
GFP
OV

F
GFP
SULT4A1
Merge
GFP
OV
G
Length (μm)
H
Width (μm)
I
Spines/10μm
J
Mushroom
Long Thin
Filopodia
Percentage of total
GFP
OV

Figure 3

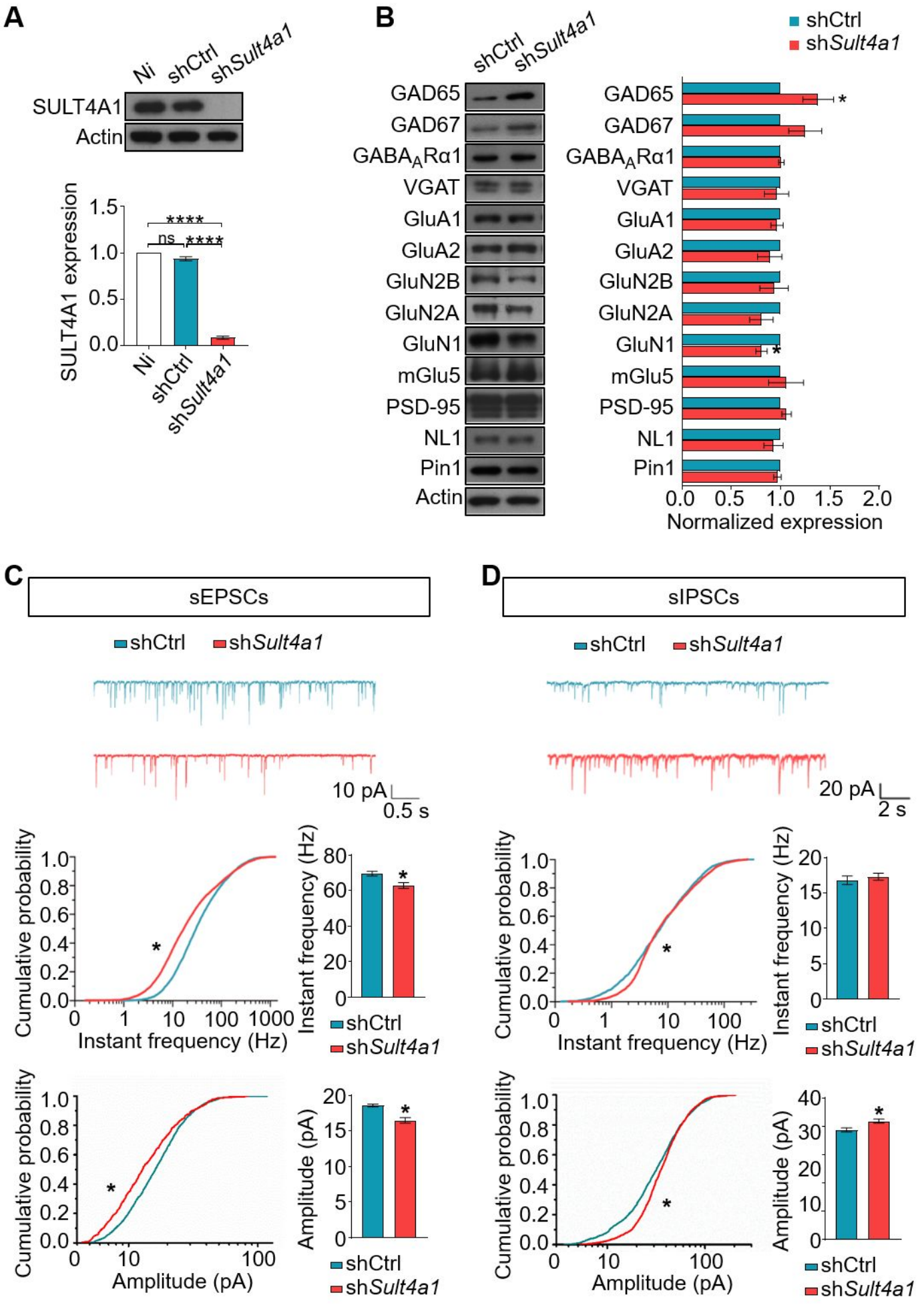
A
Ni
shCtrl
shSult4a1
SULT4A1
Actin
SULT4A1 expression
1.5
1.0
0.5
0.0
****
ns
****
Ni
shCtrl
shSult4a1
B
shCtrl
shSult4a1
shCtrl
shSult4a1
GAD65
GAD67
GABAARα1
VGAT
GluA1
GluA2
GluN2B
GluN2A
GluN1
mGlu5
PSD-95
NL1
Pin1
Actin
*
*
0.0
0.5
1.0
1.5
2.0
Normalized expression
C
sEPSCs
shCtrl
shSult4a1
10 pA
0.5 s
Cumulative probability
Instant frequency (Hz)
Instant frequency (Hz)
shCtrl
shSult4a1
Cumulative probability
Amplitude (pA)
Amplitude (pA)
shCtrl
shSult4a1
D
sIPSCs
shCtrl
shSult4a1
20 pA
2 s
Cumulative probability
Instant frequency (Hz)
Instant frequency (Hz)
shCtrl
shSult4a1
Cumulative probability
Amplitude (pA)
Amplitude (pA)
shCtrl
shSult4a1

Figure 4

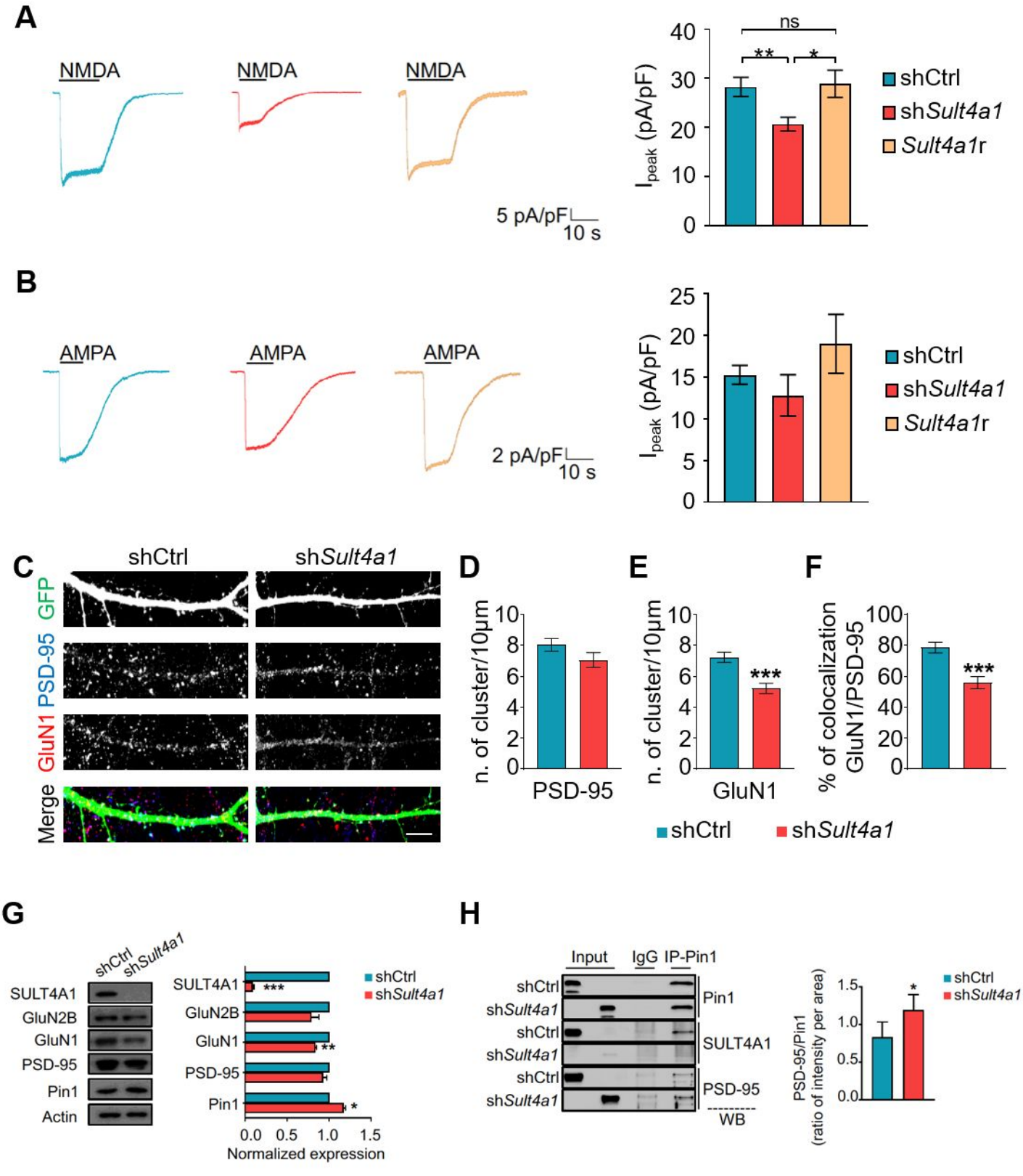
A
NMDA
NMDA
NMDA
5 pA/pF
10 s
ns
**
*
40
30
20
10
0
I_{peak} (pA/pF)
shCtrl
sh*Sult4a1*
*Sult4a1*r
B
AMPA
AMPA
AMPA
2 pA/pF
10 s
25
20
15
10
5
0
I_{peak} (pA/pF)
shCtrl
sh*Sult4a1*
*Sult4a1*r
C
shCtrl
sh*Sult4a1*
GFP
PSD-95
GluN1
Merge
D
n. of cluster/10µm
PSD-95
E
n. of cluster/10µm
***
GluN1
F
% of colocalization GluN1/PSD-95
***
shCtrl
sh*Sult4a1*
G
shCtrl
sh*Sult4a1*
SULT4A1
GluN2B
GluN1
PSD-95
Pin1
Actin
***
**
*
0.0 0.5 1.0 1.5
Normalized expression
H
Input
IgG
IP-Pin1
shCtrl
sh*Sult4a1*
Pin1
SULT4A1
PSD-95
WB
PSD-95/Pin1 (ratio of intensity per area)
*

Figure 5

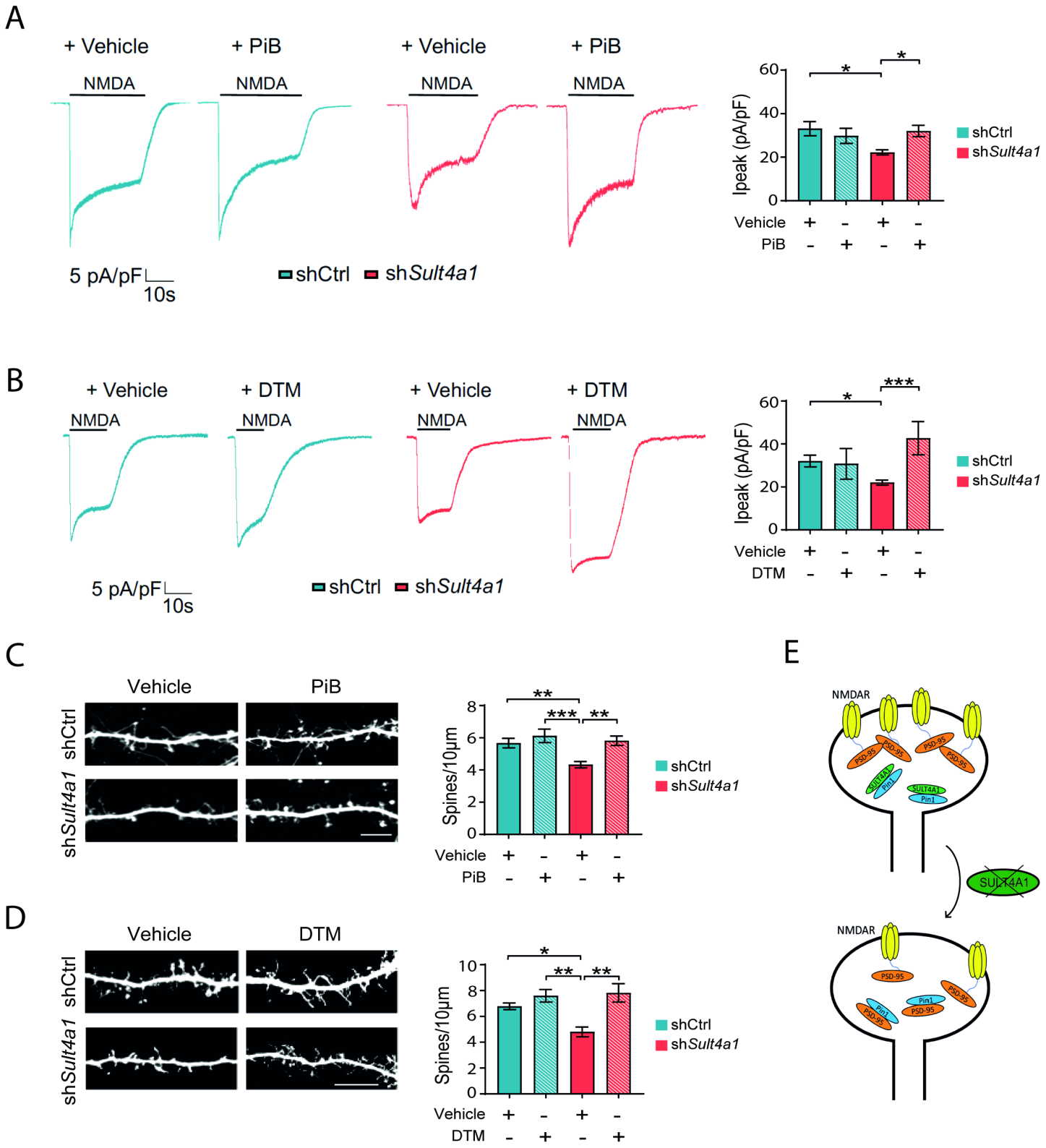
A
+ Vehicle
+ PiB
+ Vehicle
+ PiB
NMDA
NMDA
NMDA
NMDA
5 pA/pF
10s
shCtrl
shSult4a1
Ipeak (pA/pF)
60
40
20
0
*
*
Vehicle + - + -
PiB - + - +
shCtrl
shSult4a1
B
+ Vehicle
+ DTM
+ Vehicle
+ DTM
NMDA
NMDA
NMDA
NMDA
5 pA/pF
10s
shCtrl
shSult4a1
Ipeak (pA/pF)
60
40
20
0
*
***
Vehicle + - + -
DTM - + - +
shCtrl
shSult4a1
C
Vehicle
PiB
shCtrl
shSult4a1
Spines/10µm
8
6
4
2
0
**
***
**
Vehicle + - + -
PiB - + - +
shCtrl
shSult4a1
D
Vehicle
DTM
shCtrl
shSult4a1
Spines/10µm
10
8
6
4
2
0
*
**
**
Vehicle + - + -
DTM - + - +
shCtrl
shSult4a1
E
NMDAR
PSD-95
SULT4A1
Pin1
SULT4A1
NMDAR
PSD-95
Pin1

Figure 6

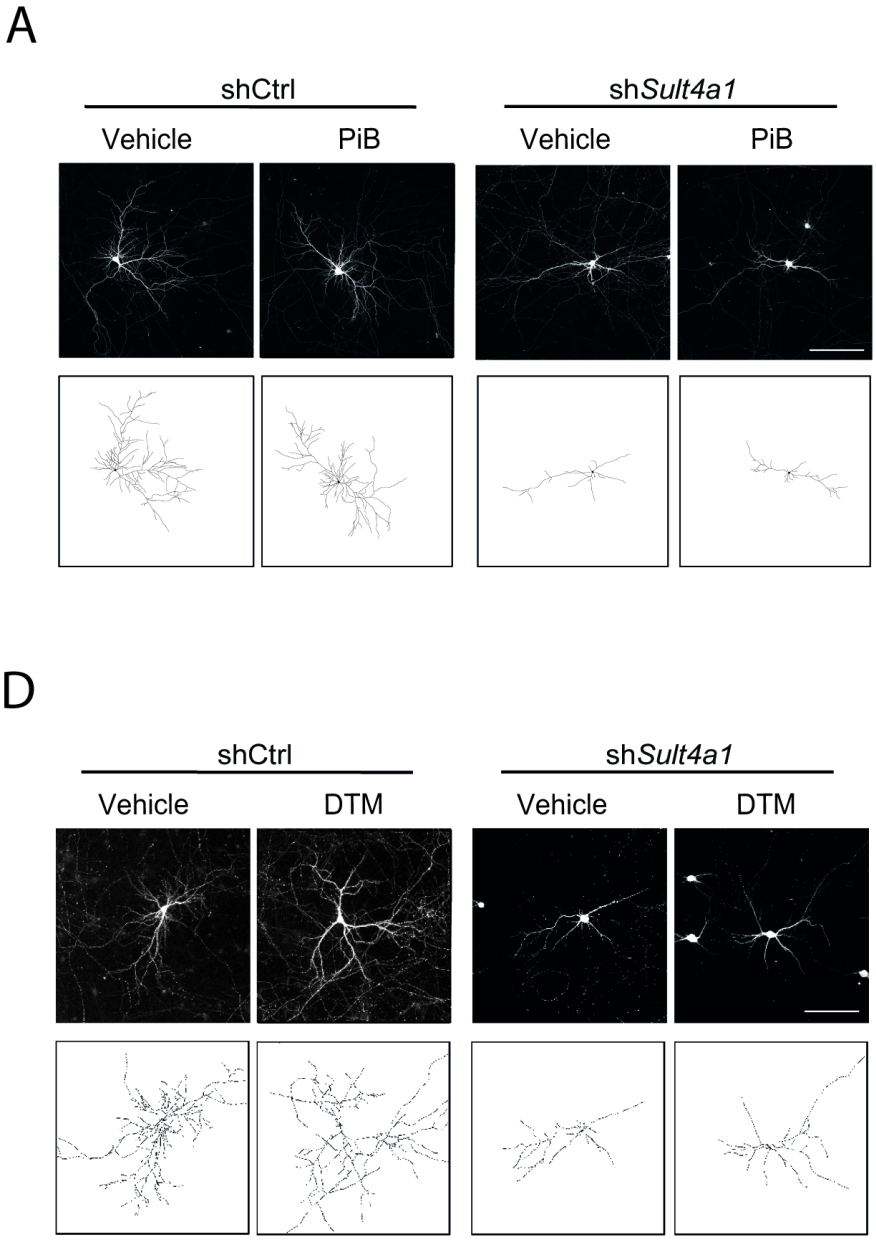
A
shCtrl
shSult4a1
Vehicle
PiB
Vehicle
PiB
B
Intersections
Distance from soma (μm)
shCtrl+Vehicle
shCtrl+PiB
C
Intersections
Distance from soma (μm)
shSult4a1+Vehicle
shSult4a1+PiB
D
shCtrl
shSult4a1
Vehicle
DTM
Vehicle
DTM
E
Intersections
Distance from soma (μm)
shCtrl+Vehicle
shCtrl+DTM
F
Intersections
Distance from soma (μm)
shSult4a1+Vehicle
shSult4a1+DTM

Figure 7